ELSEVIER

Nuclear Physics A 707 (2002) 3–31

NUCLEAR PHYSICS A

www.elsevier.com/locate/npe

Detailed study of magnetic rotation in ^{196}Pb

A.K. Singh [a], N. Nenoff [a], D. Roßbach [a], A. Görgen [a,1], S. Chmel [a], F. Azaiez [b], A. Astier [c], D. Bazzacco [d], M. Belleguic [b], S. Bouneau [b], C. Bourgeois [b], N. Buforn [c], B. Cederwall [e], I. Deloncle [f], J. Domscheit [a], F. Hannachi [f], K. Hauschild [g], H. Hübel [a,*], A. Korichi [f], W. Korten [g], T. Kröll [d], Y. LeCoz [g], A. Lopez-Martens [f], R. Lucas [g], S. Lunardi [d], H.J. Maier [h], E. Mergel [a], M. Meyer [c], C.M. Petrache [d,2], N. Redon [c], P. Reiter [h], C. Rossi-Alvarez [d], G. Schönwaßer [a], O. Stezowski [c], P.G. Thirolf [h], A.N. Wilson [i,3]

[a] *Institut für Strahlen- und Kernphysik, Universität Bonn, Nussallee 14-16, D-53115 Bonn, Germany*
[b] *IPN Orsay, IN2P3/CNRS, F-91406 Orsay, France*
[c] *IPN Lyon, IN2P3/CNRS, Université Lyon-1, F-69622 Villeurbanne, France*
[d] *Dipartimento di Fisica and INFN, Univ. di Padova, I-35131 Padova, Italy*
[e] *Department of Physics, Royal Institute of Technology, Roslagstullsbacken 21, S-106 91 Stockholm, Sweden*
[f] *CSNSM Orsay, IN2P3/CNRS, F-91405 Orsay, France*
[g] *CEA Saclay, DAPNIA/SPhN, F-91191 Gif-sur-Yvette, France*
[h] *Sektion Physik, Ludwig-Maximilians-Universität München, Am Coulombwall 1, D-85748 Garching, Germany*
[i] *Department of Physics, University of York, York YO10 5DD, UK*

Received 22 February 2002; accepted 28 March 2002

Abstract

High-spin states in ^{196}Pb have been populated in two different heavy-ion-induced reactions using thin and Au-backed targets, respectively. Gamma-ray coincidences were measured using the EUROBALL spectrometer array. Five new magnetic-rotational bands have been found. The previously known four bands have been extended and some of their levels have been reordered. With one exception, all the bands have been connected to lower-lying states and excitation energies, spins

* Corresponding author.
E-mail address: hubel@iskp.uni-bonn.de (H. Hübel).

[1] Present address: Nuclear Science Division, Lawrence Berkeley National Laboratory, Berkeley, CA 94720, USA.

[2] Present address: Department of Mathematics and Physics, University of Camerino, I-62032 Camerino, Italy.

[3] Present address: Department of Nuclear Physics, RSPhS, ANU, Canberra, ACT 0200, Australia.

0375-9474/02/$ – see front matter
PII: S0375-9474(02)00966-1

and parities have been determined. From the systematic properties of the bands and from comparison to tilted-axis cranking calculations, arguments for configuration assignments to the bands are derived. It is suggested that the bands are based on proton 11^- and 8^+ particle states coupled to various neutron–hole excitations.

PACS: 21.10.Re; 21.60.Ev; 23.20.Lv; 27.80+w

Keywords: NUCLEAR REACTIONS ^{186}W(^{16}O, 6n), $E = 110$ MeV; ^{170}Er(^{30}Si, 4n)^{196}Pb, $E = 144$ MeV; Measured $\gamma\gamma$-coincidences, E_γ, I_γ, DCO ratios, linear polarization. ^{196}Pb deduced levels, magnetic dipole bands. Shears bands, magnetic rotation, tilted-axis cranking calculations

1. Introduction

Magnetic rotation was first discovered in Pb isotopes and is now a well established mode of nuclear excitation. In many near-spherical nuclei [1–3] rotational-like cascades of strongly enhanced magnetic dipole (M1) transitions have been observed. Similar to the long-known rotation of a deformed charge distribution which we might call 'electric rotation', magnetic rotation occurs when the symmetry is broken by the current distributions of a few high-spin particles and holes outside a spherical core [4,5]. These currents lead to a large component of the magnetic dipole moment perpendicular to the total angular momentum and generate the enhanced M1 radiation.

In experiments carried out with small γ-ray spectrometer array, many of the M1 bands, in particular, in the Pb isotopes, could not be connected to lower-lying known states. Therefore, their excitation energies, spins and parities are not established. Without the knowledge of these quantities definite configuration assignments are difficult or impossible to make. Thus, up to now, the structure of many of the magnetic rotational (MR) bands remains unknown.

In this work, we report on the results of two experiments, carried out with the EUROBALL γ-ray spectrometer array [6], to investigate high-spin states in ^{196}Pb. In addition to the previously established four MR bands [7–9], we have identified five new M1 sequences. In the previous work, only one of the bands was linked to lower-lying levels. In our work, we have established these connections for all but one of the bands. In addition, the previously known bands have been extended to higher spins and some of their levels have been reordered. Furthermore, the normal scheme of irregularly spaced energy levels has been substantially extended.

In the following two sections the experimental procedure and the results are described. The structure of the MR bands is discussed and a comparison to calculations within the framework of the tilted-axis cranking (TAC) model [10] is presented in the last section.

2. Experimental procedure

Two experiments were performed to investigate high-spin states of ^{196}Pb using the EUROBALL γ-ray spectrometer array [6]. In the first experiment, excited states in ^{196}Pb were populated in the ^{186}W(^{16}O, 6n) reaction at a beam energy of 110 MeV, the beam

being provided by the Tandem accelerator at the Legnaro National Laboratory. The target consisted of a stack of two isotopically enriched foils with a thickness of 0.4 mg/cm^2 each. At the time of the experiment, the EUROBALL-III spectrometer consisted of 28 Compton-suppressed tapered Ge detectors, 25 Clover and 13 Cluster composite detectors [6]. Some of the individual Ge crystals were missing or not functioning properly during the experiment, so that out of the 239 Ge crystals of the full array 206 could be used. The requirement to write an event to tape was that at least 6 Ge crystals before Compton suppression show a coincidence. In the presorting of the data, Compton suppression, pile-up rejection, gain matching and add-back for the Ge detectors were performed and a prompt time gate was set. This resulted in a total of 2.3×10^9 three- and higher-fold (and 1.3×10^9 four- and higher-fold) coincidences.

In the second experiment, high-spin states were populated using the reaction ^{170}Er(^{30}Si, 4n)^{196}Pb at a beam energy of 144 MeV. The beam was obtained from the Vivitron Tandem accelerator at the Institut de Recherches Subatomiques at Strasbourg. The target was a 1.65 mg/cm^2 thick ^{170}Er foil backed by Au of 6.64 mg/cm^2 thickness. The EUROBALL-IV spectrometer array was used to measure γ-ray coincidences. In addition to the 26 clover, 15 cluster and 30 tapered Ge detectors, it was equipped with an 'inner ball' comprising 210 BGO scintillation detectors, which served as a multiplicity filter to enhance the selection of high-spin events. At the time of experiment, nine Ge detector crystals were not working properly and, therefore, the final number of Ge crystals available for the off-line analysis was 230. The minimum requirement for writing an event to tape was that at least four Ge crystals and five BGO elements were in coincidence. After the presorting of the data in which gain matching, Compton suppression, pile-up suppression and add-back for the composite detectors was carried out and a prompt time gate was set a total of 1.1×10^9 events of three- and higher-fold coincidences remained for subsequent analysis.

The coincidence events were unpacked and sorted into three- and four-dimensional arrays, cubes and hypercubes, respectively. To look for the weak linking transitions of the different bands, several gated E_γ–E_γ matrices were formed by setting gates on γ-ray transitions of the corresponding bands.

Two E_γ–E_γ matrices were sorted to obtain information on directional correlations from oriented states (DCO ratios). One matrix was created with the events detected in all the tapered and Cluster detectors at forward and backward angles [6], respectively, on one axis and all detectors on the other axis. A second matrix was sorted with the events detected in the Clover detectors, which are close to 90°, on one axis and all detectors on the other axis. The DCO ratio for a particular γ-ray transition was obtained by setting gates on unmixed stretched transitions of known multipolarity in the two matrices.

The Clover detectors of the EUROBALL spectrometer array were used to determine the linear polarization of γ-rays. Details about linear polarization measurements with the Clover detectors can be found, e.g., in Refs. [11,12]. The reference plane of each γ ray is spanned by the beam direction and by the emission direction of the γ ray. Compton-scattered events in neighboring pairs of Ge crystals of the Clover detectors, scattered horizontally and vertically to the reference plane, are analyzed separately. Two E_γ–E_γ matrices were created with either horizontally or vertically scattered γ rays incremented on one axis and the remaining γ rays of the event incremented on the other axis. Such

pairs of matrices were sorted with gates on uncontaminated γ-ray transitions from different MR bands. The linear polarization asymmetry ratio

$$A(E_\gamma) = \frac{I_v(E_\gamma) - I_h(E_\gamma)}{I_v(E_\gamma) + I_h(E_\gamma)}$$

is obtained by setting gates on γ-ray transitions in the two matrices. Here, I_v and I_h are the intensities of vertically and horizontally scattered γ rays of energy E_γ, respectively. Differences in the detection efficiencies of the individual crystals of the Clover detectors are small and are assumed to cancel out over the total of 26 detectors. The linear polarization P can be calculated from this asymmetry ratio by $P = A(E_\gamma)/Q(E_\gamma)$, where $Q(E_\gamma)$ is the polarization sensitivity of the polarimeter. For point-like detectors this quantity can be calculated by using Klein–Nishina formula [13]. For finite crystal-size detectors it is obtained by introducing a scaling factor to that for point-like detectors. Details about the linear polarization analysis of the same data set, but related to superdeformed bands, can be found in the Ref. [14]. The polarization asymmetry for unmixed stretched magnetic transitions is negative, whereas for electric transitions it is positive. The polarization asymmetry results of the γ rays linking MR bands to low-lying levels have been used to assign their parities.

3. Experimental results

The level scheme of ^{196}Pb, which is shown in Fig. 1, has been constructed using coincidence relationships and transition intensities. Spins and parities of the levels have been assigned on the basis of the DCO ratios and the linear polarization of the γ-ray transitions, respectively. These data are summarized in Tables 1 and 2. The lower part of the level scheme, below the 12^+ isomeric state, has been adopted from previous work [15,16]. Intensities and DCO ratios for the γ rays below this level could not be measured due to its long lifetime. The lifetimes (see Fig. 1) of the isomeric states have also been taken from the previous work [15,16].

The analysis of our data revealed five new M1 bands (labeled band 5 to 9 in Fig. 1) in addition to the four previously known bands [7–9]. Some transitions within the bands have been reordered on the basis of the intensity pattern. Several new E2 crossover transitions have also been observed which determine the ordering of the γ-ray transitions within the bands. All the bands, except band 7, are connected to low-lying states. Although our work was focused on the MR bands, the normal level scheme has also been extended.

In the following, a brief summary is given of the evidence that establishes the nine MR bands in the level scheme of ^{196}Pb.

3.1. Band 1

A summed γ-ray coincidence spectrum with double gates on several clean transitions of band 1 is shown in Fig. 2. With an intensity of almost 30% of that of the 958.7 keV transition (see Table 1) this band has the highest intensity of all the MR bands observed in ^{196}Pb. It has been reported in previous work [7–9], however, it was not connected to

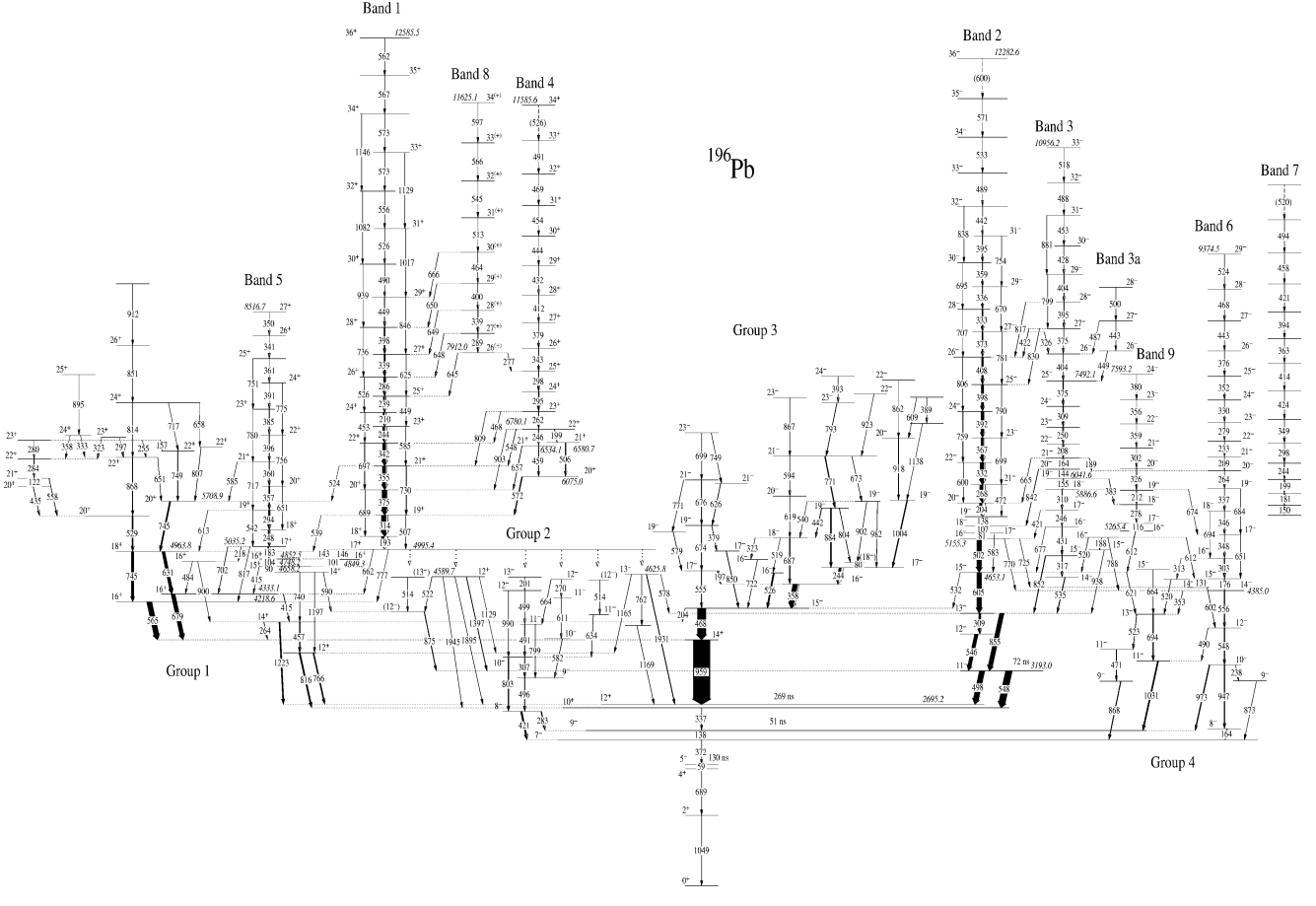

Fig. 1. The level scheme of ^{196}Pb. The bands are numbered according to their intensities.

Table 1
Energies, intensities, DCO ratios and multipolarity and spin assignments of γ-ray transitions of ^{196}Pb. The uncertainties in the energies of the γ-rays are between 0.2 and 0.6 keV depending on their intensity. The intensities are normalized to the 958.7 keV transition with $I_\gamma = 1000$. The DCO ratios are normalized to stretched E2 transitions

	Energy E_γ (keV)	Intensity I_γ (rel.)	R_{DCO}	Multipolarity	Excitation E_i (keV)	Assignment $I_i^\pi \to I_f^\pi$
Band 1	192.7	150(14)	0.44(5)	M1	5188.1	$18^+ \to 17^+$
	209.8	89(12)	0.46(6)	M1	7027.5	$24^+ \to 23^+$
	239.4	85(13)	0.46(6)	M1	7266.9	$25^+ \to 24^+$
	243.6	128(14)	0.47(5)	M1	6817.7	$23^+ \to 22^+$
	286.1	72(11)	0.43(6)	M1	7553.0	$26^+ \to 25^+$
	314.5	274(25)	0.45(4)	M1	5502.6	$19^+ \to 18^+$
	338.7	68(10)	0.42(7)	M1	7891.7	$27^+ \to 26^+$
	341.6	189(18)	0.48(5)	M1	6574.1	$22^+ \to 21^+$
	355.3	202(18)	0.46(4)	M1	6232.5	$21^+ \to 20^+$
	374.6	248(25)	0.45(5)	M1	5877.2	$20^+ \to 19^+$
	397.7	56(8)	0.41(7)	M1	8289.4	$28^+ \to 27^+$
	448.7	24(5)	0.45(8)	M1	8738.1	$29^+ \to 28^+$
	449.2[a]	–	–	E2	7266.9	$25^+ \to 23^+$
	453.4	3.0(12)	–	E2	7027.5	$24^+ \to 22^+$
	490.2	13(3)	0.42(9)	M1	9228.3	$30^+ \to 29^+$
	507.2	13(4)	–	E2	5502.6	$19^+ \to 17^+$
	525.5[a]	–	–	E2	7553.0	$26^+ \to 24^+$
	526.4	8.9(16)	0.39(10)	M1	9754.7	$31^+ \to 30^+$
	555.9	5.3(18)	0.50(12)	M1	10310.6	$32^+ \to 31^+$
	562.5	1.7(9)	–	M1	12585.5	$36^+ \to 35^+$
	566.7	2.8(12)	–	M1	12023.0	$35^+ \to 34^+$
	572.6 }	5.1(18)[b]	0.41(12)[b]	M1	11456.3	$34^+ \to 33^+$
	573.1 }			M1	10883.7	$33^+ \to 32^+$
	585.2	9.5(26)	1.16(19)	E2	6817.7	$23^+ \to 21^+$
	624.8	4.7(16)	–	E2	7891.7	$27^+ \to 25^+$
	689.1	27(6)	0.92(9)	E2	5877.2	$20^+ \to 18^+$
	696.9	28(6)	1.06(9)	E2	6574.1	$22^+ \to 20^+$
	729.9	30(5)	1.06(9)	E2	6232.5	$21^+ \to 19^+$
	736.4	7.0(15)	0.91(15)	E2	8289.4	$28^+ \to 26^+$
	846.4	4.9(12)	0.80(21)	E2	8738.1	$29^+ \to 27^+$
	938.9	2.6(8)	–	E2	9228.1	$30^+ \to 28^+$
	1016.6	2.1(8)	–	E2	9754.7	$31^+ \to 29^+$
	1082.3	2.0(9)	–	E2	10310.6	$32^+ \to 30^+$
	1129.0	1.7(7)	–	E2	10883.7	$33^+ \to 31^+$
	1145.7	< 1	–	E2	11456.3	$34^+ \to 32^+$
Decay of band 1	142.9	9.3(23)	0.47(8)	M1	4995.4	$17^+ \to 16^+$
	146.1	5.2(14)	0.55(12)	M1	4995.4	$17^+ \to 16^+$
	523.6	2.6(7)	0.59(17)	M1	6232.5	$21^+ \to 20^+$
	538.8	3.0(9)	0.76(18)	M1	5502.6	$19^+ \to 18^+$
	662.3	4.5(10)	0.45(10)	M1	4995.4	$17^+ \to 16^+$
	776.8	2.7(8)	0.52(17)	M1	4995.4	$17^+ \to 16^+$
Band 2	80.7	–	–	M1	5236.0	$17^- \to 16^-$
	106.9	40(9)	0.43(6)	M1	5342.9	$18^- \to 17^-$
	138.0	76(11)	0.48(5)	M1	5480.9	$19^- \to 18^-$
	203.9	160(19)	0.47(5)	M1	5684.8	$20^- \to 19^-$

Table 1 (*continued*)

	Energy E_γ (keV)	Intensity I_γ (rel.)	R_{DCO}	Multipolarity	Excitation E_i (keV)	Assignment $I_i^\pi \rightarrow I_f^\pi$
	267.8	206(24)	0.50(4)	M1	5952.6	$21^- \rightarrow 20^-$
	331.8	209(38)	0.53(5)	M1	6284.4	$22^- \rightarrow 21^-$
	333.5	38(6)	0.49(9)	M1	8556.3	$28^- \rightarrow 27^-$
	336.5	27(6)	0.51(10)	M1	8892.8	$29^- \rightarrow 28^-$
	358.5	18(4)	0.54(9)	M1	9251.3	$30^- \rightarrow 29^-$
	367.0	155(18)	0.46(5)	M1	6651.4	$23^- \rightarrow 22^-$
	373.4	51(8)	0.44(8)	M1	8222.8	$27^- \rightarrow 26^-$
	392.2	140(18)	0.49(5)	M1	7043.6	$24^- \rightarrow 23^-$
	395.5	10.4(25)	0.46(10)	M1	9646.8	$31^- \rightarrow 30^-$
	397.7	116(15)	0.43(6)	M1	7441.3	$25^- \rightarrow 24^-$
	408.3	83(11)	0.44(6)	M1	7849.4	$26^- \rightarrow 25^-$
	442.1	8.2(21)	0.40(10)	M1	10088.9	$32^- \rightarrow 31^-$
	471.7	7.4(22)	–	E2	5952.6	$21^- \rightarrow 19^-$
	489.4	4.3(13)	–	M1	10578.3	$33^- \rightarrow 32^-$
	533.5	2.6(10)	–	M1	11111.8	$34^- \rightarrow 33^-$
	571.3	1.4(6)	–	M1	11683.1	$35^- \rightarrow 34^-$
	599.5	< 1	–	M1	12282.6	$36^- \rightarrow 35^-$
	599.6	9.2(32)	–	E2	6284.4	$22^- \rightarrow 20^-$
	670.0	2.5(11)	–	E2	8892.8	$29^- \rightarrow 27^-$
	695.0	2.7(11)	–	E2	9251.3	$30^- \rightarrow 28^-$
	698.8	18(4)	0.98(14)	E2	6651.4	$23^- \rightarrow 21^-$
	706.9	3.3(9)	0.85(24)	E2	8556.3	$28^- \rightarrow 26^-$
	754.0	2.1(7)	–	E2	9646.8	$31^- \rightarrow 29^-$
	759.2	22(6)	1.36(21)	E2	7043.6	$24^- \rightarrow 22^-$
	781.5	6.8(22)	1.24(27)	E2	8222.8	$27^- \rightarrow 25^-$
	789.9	23(7)	0.93(10)	E2	7441.3	$25^- \rightarrow 23^-$
	805.8	19(5)	1.09(14)	E2	7849.4	$26^- \rightarrow 24^-$
	837.6	2.5(12)	–	E2	10088.9	$32^- \rightarrow 30^-$
Decay of band 2	582.9	9.7(16)	0.90(17)	E2	5236.0	$17^- \rightarrow 15^-$
	326.3	9(3)	0.46(10)	M1	8222.8	$27^- \rightarrow 26^-$
Band 3	143.7	21(6)	0.44(8)	M1	6185.3	$20^- \rightarrow 19^-$
	155.0	13(3)	0.44(12)	M1	6041.6	$19^- \rightarrow 18^-$
	164.1	27(7)	0.50(8)	M1	6349.4	$21^- \rightarrow 20^-$
	208.3	47(8)	0.47(6)	M1	6557.7	$22^- \rightarrow 21^-$
	250.2	54(9)	0.46(6)	M1	6807.9	$23^- \rightarrow 22^-$
	309.1	48(11)[b]	0.55(8)[b]	M1	7117.0	$24^- \rightarrow 23^-$
	374.8	45(9)[b]	0.47(6)[b]	M1	8271.3	$27^- \rightarrow 26^-$
	375.1			M1	7492.1	$25^- \rightarrow 24^-$
	395.0	17(5)	0.37(8)	M1	8666.3	$28^- \rightarrow 27^-$
	404.1	14(4)	0.40(8)	M1	9070.4	$29^- \rightarrow 28^-$
	404.4	22(5)	0.39(8)	M1	7896.5	$26^- \rightarrow 25^-$
	428.0	10(3)	0.37(9)	M1	9498.4	$30^- \rightarrow 29^-$
	452.6	5.6(19)	0.46(13)	M1	9951.0	$31^- \rightarrow 30^-$
	487.6	4.0(13)	–	M1	10438.6	$32^- \rightarrow 31^-$
	517.6	2.3(9)	–	M1	10956.2	$33^- \rightarrow 32^-$
	799.1	2.5(9)	–	E2	9070.4	$29^- \rightarrow 27^-$
	880.6	1.6(8)	–	E2	9951.0	$31^- \rightarrow 29^-$
Decay of band 3	189.1	8.7(17)	0.38(9)	M1	6349.4	$21^- \rightarrow 20^-$
	383.0	13(3)	0.48(10)	M1	6041.6	$19^- \rightarrow 18^-$

Table 1 (*continued*)

	Energy E_γ (keV)	Intensity I_γ (rel.)	R_{DCO}	Multipolarity	Excitation E_i (keV)	Assignment $I_i^\pi \rightarrow I_f^\pi$
	421.9	25(6)	0.47(7)	M1	8271.3	$27^- \rightarrow 26^-$
	664.7	4.3(13)	–	M1	6349.4	$21^- \rightarrow 20^-$
	816.9	4.2(14)	1.04(18)	E2	8666.3	$28^- \rightarrow 26^-$
	830.0	5.3(15)	0.96(17)	E2	8271.3	$27^- \rightarrow 25^-$
	842.4	19(5)	0.87(20)	E2	6185.3	$20^- \rightarrow 18^-$
Band 3a	442.7	5.2(16)	0.44(12)	M1	8383.6	$27^- \rightarrow 26^-$
	448.9	8.4(22)	0.39(9)	M1	7940.9	$26^- \rightarrow 25^-$
	499.5	1.8(8)	–	M1	8884.1	$28^- \rightarrow 27^-$
Decay of band 3a	487.1	3.2(12)	–	M1	8383.6	$27^- \rightarrow 26^-$
Band 4	261.7	15(3)	0.50(9)	M1	7041.8	$23^+ \rightarrow 22^+$
	294.9	35(6)	0.49(7)	M1	7336.7	$24^+ \rightarrow 23^+$
	297.9	23(4)	0.40(8)	M1	7634.6	$25^+ \rightarrow 24^+$
	342.9	19(3)	0.44(8)	M1	7977.5	$26^+ \rightarrow 25^+$
	379.4	15(3)	0.44(9)	M1	8356.9	$27^+ \rightarrow 26^+$
	412.3	10.2(19)	0.40(10)	M1	8769.2	$28^+ \rightarrow 27^+$
	432.5	6.6(12)	0.37(11)	M1	9201.7	$29^+ \rightarrow 28^+$
	443.7	4.8(8)	0.42(14)	M1	9645.4	$30^+ \rightarrow 29^+$
	454.0	3.6(6)	–	M1	10099.4	$31^+ \rightarrow 30^+$
	468.6	2.2(8)	–	M1	10568.0	$32^+ \rightarrow 31^+$
	491.4	1.3(5)	–	M1	11059.4	$33^+ \rightarrow 32^+$
	526.2	< 1	–	M1	11585.6	$34^+ \rightarrow 33^+$
Decay of band 4	199.4	7.3(18)	0.61(16)	M1	6780.1	$22^+ \rightarrow 21^+$
	246.0	10.1(27)	0.52(13)	M1	6780.1	$22^+ \rightarrow 21^+$
	459.1	13(4)	0.72(15)	M1	6534.1	$21^+ \rightarrow 20^+$
	467.7	8(3)	–	M1	7041.8	$23^+ \rightarrow 22^+$
	505.7	11(5)	0.46(12)	M1	6580.7	$21^+ \rightarrow 20^+$
	547.6	9(3)	–	M1	6780.1	$22^+ \rightarrow 21^+$
	572.4	30(8)	0.38(8)	M1	6075.0	$20^+ \rightarrow 19^+$
	656.9	6.2(18)	0.62(25)	M1	6534.1	$21^+ \rightarrow 20^+$
	809.3	7.8(16)	0.85(22)	E2	7041.8	$23^+ \rightarrow 21^+$
	903.0	6.3(14)	1.08(24)	E2	6780.1	$22^+ \rightarrow 20^+$
Band 5	90.0	–	–	M1	4748.2	$15^+ \rightarrow 14^+$
	104.3	8.9(27)	0.51(13)	M1	4852.5	$16^+ \rightarrow 15^+$
	182.7	59(9)	0.46(7)	M1	5035.2	$17^+ \rightarrow 16^+$
	248.1	71(10)	0.44(7)	M1	5283.3	$18^+ \rightarrow 17^+$
	293.9	60(8)	0.45(7)	M1	5577.2	$19^+ \rightarrow 18^+$
	340.7	5.5(15)	0.52(9)	M1	8166.3	$26^+ \rightarrow 25^+$
	350.4	3.6(12)	0.43(9)	M1	8516.7	$27^+ \rightarrow 26^+$
	356.8	46(9)	0.49(8)	M1	5934.0	$20^+ \rightarrow 19^+$
	360.1 }	37(11)[b]	0.45(9)[b]	M1	6294.1	$21^+ \rightarrow 20^+$
	360.6 }			M1	7825.6	$25^+ \rightarrow 24^+$
	384.7	15(3)	0.40(11)	M1	7074.4	$23^+ \rightarrow 22^+$
	390.6	11(24)	0.39(11)	M1	7465.0	$24^+ \rightarrow 23^+$
	395.6	18(4)	0.41(9)	M1	6689.7	$22^+ \rightarrow 21^+$
	542.0	5.2(18)	0.93(17)	E2	5577.2	$19^+ \rightarrow 17^+$
	650.7	6.2(23)	0.89(15)	E2	5934.0	$20^+ \rightarrow 18^+$
	716.9	6.6(18)	0.88(17)	E2	6294.1	$21^+ \rightarrow 19^+$
	751.2	1.4(7)	–	E2	7825.6	$25^+ \rightarrow 23^+$
	755.7	3.0(10)	1.06(19)	E2	6689.7	$22^+ \rightarrow 20^+$

Table 1 (*continued*)

	Energy E_γ (keV)	Intensity I_γ (rel.)	R_{DCO}	Multipolarity	Excitation E_i (keV)	Assignment $I_i^\pi \rightarrow I_f^\pi$
	775.3	2.4(9)	0.90(22)	E2	7465.0	$24^+ \rightarrow 22^+$
	780.3	3.4(11)	1.02(21)	E2	7074.4	$23^+ \rightarrow 21^+$
Decay of band 5	217.7	9.2(23)	0.49(12)	M1	5035.2	$17^+ \rightarrow 16^+$
	585.2	6.8(18)	0.38(12)	M1	6294.1	$21^+ \rightarrow 20^+$
	613.4	8.2(21)	0.44(11)	M1	5577.2	$19^+ \rightarrow 18^+$
	702.1	15(3)	0.44(9)	M1	5035.2	$17^+ \rightarrow 16^+$
	816.6	7.4(19)	0.60(15)	M1	5035.2	$17^+ \rightarrow 16^+$
Band 6	176.2	18(4)	0.46(9)	M1	4561.2	$15^- \rightarrow 14^-$
	209.0	7.5(18)	0.49(12)	M1	6369.3	$21^- \rightarrow 20^-$
	232.8	5.1(15)	0.50(14)	M1	6602.1	$22^- \rightarrow 21^-$
	264.1	10(3)	0.41(11)	M1	6160.3	$20^- \rightarrow 19^-$
	279.2	3.5(12)	0.48(15)	M1	6881.3	$23^- \rightarrow 22^-$
	303.2	26(6)	0.44(8)	M1	4864.4	$16^- \rightarrow 15^-$
	330.4	2.6(8)	0.43(15)	M1	7211.7	$24^- \rightarrow 23^-$
	337.4	11(3)	–	M1	5896.2	$19^- \rightarrow 18^-$
	346.5	15(6)	0.45(9)[c]	M1	5558.8	$18^- \rightarrow 17^-$
	347.9	18(5)		M1	5212.3	$17^- \rightarrow 16^-$
	352.3	2.0(6)	0.38(15)	M1	7564.0	$25^- \rightarrow 24^-$
	376.5	1.7(6)	–	M1	7940.5	$26^- \rightarrow 25^-$
	442.6	1.2(5)	–	M1	8383.1	$27^- \rightarrow 26^-$
	467.7	< 1	–	M1	8850.8	$28^- \rightarrow 27^-$
	523.7	< 1	–	M1	9374.5	$29^- \rightarrow 28^-$
	651.1	2.8(9)	–	E2	5212.3	$17^- \rightarrow 15^-$
	683.9	3.2(8)	0.89(24)	E2	5896.2	$19^- \rightarrow 17^-$
	694.4	2.8(8)	0.89(25)	E2	5558.8	$18^- \rightarrow 16^-$
Decay of band 6	130.6	1.5(6)	–	M1	4561.2	$15^- \rightarrow 14^-$
	312.8	1.8(6)	–	–	4864.4	$16^- \rightarrow$ –
Band 7	150.3	6.4(16)	0.42(10)	M1		
	181.0	16(3)	0.44(9)	M1		
	198.6	19(4)	0.41(8)	M1		
	244.3	14(3)	0.48(9)	M1		
	297.7	10.3(23)	0.45(9)	M1		
	348.8	7.7(18)	0.38(10)	M1		
	362.8	2.3(8)	0.40(11)	M1		
	393.6	1.7(6)	0.45(13)	M1		
	413.7	3.3(10)	0.53(15)	M1		
	420.8	1.3(5)	–	M1		
	423.7	5.1(14)	0.46(12)	M1		
	457.8	1.0(5)	–	M1		
	493.5	< 1	–	M1		
	520.2	< 1	–	M1		
Band 8	289.0	18(4)	0.53(9)	M1	8201.0	$27^{(+)} \rightarrow 26^{(+)}$
	339.3	16(4)	0.39(10)	M1	8540.3	$28^{(+)} \rightarrow 27^{(+)}$
	399.5	12(3)	0.43(9)	M1	8939.8	$29^{(+)} \rightarrow 28^{(+)}$
	464.1	8.1(18)	0.41(10)	M1	9403.9	$30^{(+)} \rightarrow 29^{(+)}$
	513.2	5.7(14)	0.42(10)	M1	9917.1	$31^{(+)} \rightarrow 30^{(+)}$
	544.6	3.8(10)	–	M1	10461.7	$32^{(+)} \rightarrow 31^{(+)}$
	566.2	2.4(7)	–	M1	11027.9	$33^{(+)} \rightarrow 32^{(+)}$
	597.2	1.3(5)	–	M1	11625.1	$34^{(+)} \rightarrow 33^{(+)}$

Table 1 (*continued*)

	Energy E_γ (keV)	Intensity I_γ (rel.)	$R_{\rm DCO}$	Multipolarity	Excitation E_i (keV)	Assignment $I_i^\pi \to I_f^\pi$
Decay of band 8	277.4	6.4(15)	0.43(10)	(M1)	7912.0	$26^{(+)} \to 25^+$
	645.1	1.9(8)	–	M1	7912.0	$26^{(+)} \to 25^+$
	648.0			M1	8201.0	$27^{(+)} \to 26^+$
	648.6	3.6(15)[d]	–	M1	8540.3	$28^{(+)} \to 27^+$
	650.4			M1	8939.8	$29^{(+)} \to 28^+$
	665.8	1.7(5)	–	M1	9403.9	$30^{(+)} \to 29^+$
Band 9	115.7	5.2(14)	0.39(12)	M1	5381.1	$17^- \to 16^-$
	212.0	6.1(15)	0.42(12)	M1	5870.6	$19^- \to 18^-$
	277.5	15(3)	0.47(10)	M1	5658.6	$18^- \to 17^-$
	302.2	3.4(8)	0.47(14)	M1	6498.9	$21^- \to 20^-$
	326.1	8.3(18)	0.35(9)	M1	6196.7	$20^- \to 19^-$
	355.6	1.5(8)	–	M1	7213.5	$23^- \to 22^-$
	359.0	1.9(6)	–	M1	6857.9	$22^- \to 21^-$
	379.7	< 1	–	M1	7593.2	$24^- \to 23^-$
Decay of band 9	612.3	16(4)	0.48(9)	M1	5265.4	$16^- \to 15^-$
Group 1	101.1	2.6(9)	–	M1	4849.3	$16^+ \to 15^+$
	122.2	2.7(7)	0.38(14)	M1	6050.4	$21^+ \to 20^+$
	156.4	3.3(8)	0.28(13)	M1	6614.9	$23^+ \to 22^+$
	254.5	4.4(12)	0.33(12)	M1	6614.9	$23^+ \to 22^+$
	263.9	10(3)	0.56(16)	M1	3917.8	$14^+ \to 14^+$
	280.5	4.4(14)	0.45(13)	M1	6614.9	$23^+ \to 22^+$
	284.0	12(3)	0.64(15)	M1	6334.4	$22^+ \to 21^+$
	297.2	2.4(7)	0.61(16)	M1	6657.6	$23^+ \to 22^+$
	323.2	2.8(8)	0.50(15)	M1	6657.6	$23^+ \to 22^+$
	332.5	2.3(7)	1.02(23)	E2	6692.9	$24^+ \to 22^+$
	358.5	2.6(8)	–	E2	6692.9	$24^+ \to 22^+$
	415.1	7.0(18)	0.38(12)	M1	4748.2	$15^+ \to 16^+$
	415.3	18(4)	1.00(18)	E2	4333.1	$16^+ \to 14^+$
	435.4	15(3)	0.90(17)	M1	5928.2	$20^+ \to 20^+$
	456.6	53(12)	0.99(13)	E2	3917.8	$14^+ \to 12^+$
	484.4	4.5(13)	0.65(16)	M1	4817.5	$16^+ \to 16^+$
	529.0	66(8)	0.94(14)	E2	5492.8	$20^+ \to 18^+$
	557.6	15(3)	0.72(16)	M1	6050.4	$21^+ \to 20^+$
	564.7	296(33)	1.00	E2	4218.6	$16^+ \to 14^+$
	590.2	8.2(22)	–	(M2)	4658.2	$14^+ \to (12^-)$
	630.7	172(19)	1.02(13)	E2	4963.8	$18^+ \to 16^+$
	651.5	11(3)	1.06(22)	E2	6360.4	$22^+ \to 20^+$
	658.3	1.5(5)	–	E2	7174.3	$24^+ \to 22^+$
	679.2	233(26)	1.00	E2	4333.1	$16^+ \to 14^+$
	716.8	5.7(14)	0.87(26)	E2	7174.3	$24^+ \to 22^+$
	740.4	8.7(24)	0.82(24)	M1	4658.8	$14^+ \to 14^+$
	745.1	76(11)	1.00(14)	E2	5708.9	$20^+ \to 18^+$
	745.2	132(16)	1.02(13)	E2	4963.8	$18^+ \to 16^+$
	748.6	23(5)	1.19(19)	E2	6457.5	$22^+ \to 20^+$
	766.0	62(14)	0.65(11)	M1	3461.2	$12^+ \to 12^+$
	807.1	13(3)	0.93(22)	E2	6516.0	$22^+ \to 20^+$
	813.9	5.9(17)	1.39(36)	E2	7174.3	$24^+ \to 22^+$
	816.0	81(13)	1.08(15)	E2	3461.2	$12^+ \to 10^+$
	851.1	2.2(7)	1.12(28)	E2	8025.4	$26^+ \to 24^+$

Table 1 (*continued*)

	Energy E_γ (keV)	Intensity I_γ (rel.)	R_{DCO}	Multipolarity	Excitation E_i (keV)	Assignment $I_i^\pi \rightarrow I_f^\pi$
	867.6	20(4)	1.10(18)	E2	6360.4	$22^+ \rightarrow 20^+$
	895.1	4.4(12)	0.51(14)	M1	7588.0	$25^+ \rightarrow 24^+$
	899.7	6.8(18)	0.92(18)	E2	4817.5	$16^+ \rightarrow 14^+$
	911.9	< 1	–	–	8937.3	$- \rightarrow 26^+$
	1197.0	13(4)	1.22(24)	E2	4658.2	$14^+ \rightarrow 12^+$
	1222.6	75(11)	1.07(14)	E2	3917.8	$14^+ \rightarrow 12^+$
Group 2	201.4	4.4(13)	0.44(12)	M1	4585.8	$13^- \rightarrow 12^-$
	203.7	8.3(18)	–	E1	4121.5	$15^- \rightarrow 14^+$
	269.9	9.0(18)	0.50(9)	M1	4549.6	$12^- \rightarrow 11^-$
	283.0	29(7)	0.47(13)	M1	2590.8	$8^- \rightarrow 9^-$
	307.1	12(4)	0.51(9)	M1	3393.9	$10^- \rightarrow 9^-$
	421.2	82(12)	0.61(11)	M1	2590.8	$8^- \rightarrow 7^-$
	491.4	13(3)	0.48(14)	M1	3885.3	$11^- \rightarrow 10^-$
	496.0	35(6)	0.40(11)	M1	3086.8	$9^- \rightarrow 8^-$
	499.1	4.9(15)	–	M1	4384.4	$12^- \rightarrow 11^-$
	513.9	12(3)	0.34(11)[c]	(M1)	4581.9	$(13^-) \rightarrow 12^{(-)}$
	514.1	11(3)		(M1)	4542.3	$(12^-) \rightarrow 11^-$
	521.7	11(3)	–	E1	4589.7	$12^+ \rightarrow 12^-$
	578.2	5.8(16)	–	M1	4625.8	$13^- \rightarrow 13^-$
	582.3	14(3)	0.47(5)	M1	3669.1	$10^- \rightarrow 9^-$
	610.6	10.0(24)	0.51(18)	M1	4279.7	$11^- \rightarrow 10^-$
	634.3	12(3)	0.69(20)	M1	4028.2	$11^- \rightarrow 10^-$
	664.3	11.3(26)	–	M1	4549.6	$12^- \rightarrow 11^-$
	761.9	–	–	–	4625.8	$13^- \rightarrow -$
	798.5	9.9(24)	0.98(23)	E2	3885.3	$11^- \rightarrow 9^-$
	803.1	37(7)	0.94(14)	E2	3393.9	$10^- \rightarrow 8^-$
	875.0	33(6)	0.57(9)	M1	4068.0	$12^- \rightarrow 11^-$
	990.5	13(3)	1.04(18)	E2	4384.4	$12^- \rightarrow 10^-$
	1128.5	4.3(12)	0.63(13)	M1	4589.7	$12^+ \rightarrow 12^+$
	1164.6	8.8(20)	0.64(10)	E1	4625.8	$13^- \rightarrow 12^+$
	1168.7	–	–	–	3863.9	$- \rightarrow 12^+$
	1396.7	26(7)	0.55(8)	E1	4589.7	$12^+ \rightarrow 11^-$
	1894.5	9(3)	0.73(14)	M1	4589.7	$12^+ \rightarrow 12^+$
	1930.6	32(9)	0.38(9)	E1	4625.8	$13^- \rightarrow 12^+$
	1944.5	9(3)	1.34(21)	E2	4589.7	$12^+ \rightarrow 10^+$
Group 3	79.9	–	–	–	4803.5	$(18^-) \rightarrow 17^-$
	197.1	44(8)	0.37(6)	M1	4676.4	$17^- \rightarrow 16^-$
	244.3	146(18)	0.75(9)	M1	4723.6	$17^- \rightarrow 16^-$
	322.8	8.7(20)	0.84(24)	E2	5166.0	$18^- \rightarrow 16^-$
	357.8	282(31)	0.63(6)	M1	4479.3	$16^- \rightarrow 15^-$
	378.8	17(4)	0.90(19)	E2	5350.2	$19^- \rightarrow 17^-$
	388.7	4.2(14)	–	–	7254.3	–
	392.7	6.1(19)	0.31(7)	M1	7564.3	$24^- \rightarrow 23^-$
	441.9	25(5)	0.62(9)	M1	5607.9	$19^- \rightarrow 18^-$
	467.6	503(46)	0.60(5)	E1	4121.5	$15^- \rightarrow 14^+$
	518.6	5.8(13)	1.29(26)	E2	5166.0	$18^- \rightarrow 16^-$
	525.9	75(11)	0.50(7)	M1	4647.4	$16^- \rightarrow 15^-$
	539.7	5.7(14)	–	M1	5705.7	$19^- \rightarrow 18^-$
	554.9	36(8)	1.03(16)	E2	4676.4	$17^- \rightarrow 15^-$

Table 1 (*continued*)

	Energy E_γ (keV)	Intensity I_γ (rel.)	R_{DCO}	Multipolarity	Excitation E_i (keV)	Assignment $I_i^\pi \rightarrow I_f^\pi$
	578.6	15(3)	0.90(16)	E2	5255.0	$19^- \rightarrow 17^-$
	593.6	10(2)	0.93(19)	E2	6379.0	$21^- \rightarrow 19^-$
	608.9	6.6(17)	–	–	7254.3	$- \rightarrow 20^-$
	619.4	12(3)	0.85(19)	E2	5785.4	$20^- \rightarrow 18^-$
	625.7	21(5)	1.04(19)	E2	5975.9	$21^- \rightarrow 19^-$
	673.3	12(3)	1.05(18)[c]	(E2)	6379.0	$21^- \rightarrow (19^-)$
	673.8	29(6)		E2	5350.2	$19^- \rightarrow 17^-$
	675.8	15(4)	1.08(16)	E2	6026.0	$21^- \rightarrow 19^-$
	686.7	42(7)	1.14(16)	E2	5166.0	$18^- \rightarrow 16^-$
	699.1	10(2)	0.87(18)	E2	6725.1	$23^- \rightarrow 21^-$
	721.7	11(2)	0.42(13)	M1	4843.2	$16^- \rightarrow 15^-$
	749.2	10(3)	0.84(15)	E2	6725.1	$23^- \rightarrow 21^-$
	771.0	10(3)	–	E2	6026.0	$21^- \rightarrow 19^-$
	771.1	48(8)	1.02(14)	E2	6379.0	$21^- \rightarrow 19^-$
	792.6	20(5)	0.85(14)	E2	7171.6	$23^- \rightarrow 21^-$
	804.4	17(4)	0.45(9)	M1	5607.9	$19^- \rightarrow (18^-)$
	849.9	25(5)	0.91(15)	E2	4971.4	$17^- \rightarrow 15^-$
	862.2	5.4(16)	0.92(26)	E2	7507.6	$22^- \rightarrow 20^-$
	866.8	13(3)	0.97(18)	E2	7245.8	$23^- \rightarrow 21^-$
	884.3	56(8)	0.99(12)	E2	5607.9	$19^- \rightarrow 17^-$
	902.2	12(3)	–	(M1)	5705.7	$19^- \rightarrow (18^-)$
	917.5	11(2)	0.65(11)	M1	6645.4	$20^- \rightarrow 19^-$
	922.9	6.2(16)	0.65(16)	M1	7301.9	$22^- \rightarrow 21^-$
	958.7	1000	1.00	E2	3653.9	$14^+ \rightarrow 12^+$
	982.1	16(4)	0.84(18)	E2	5705.7	$19^- \rightarrow 17^-$
	1004.3	53(7)	1.20(16)	E2	5727.9	$19^- \rightarrow 17^-$
	1137.7	5.6(17)	–	–	6865.6	$- \rightarrow 19^-$
Group 4	164.4	31(8)	0.55(7)	M1	2334.0	$8^- \rightarrow 7^-$
	187.5	3.3(11)	–	M1	5173.5	$16^- \rightarrow 15^-$
	238.0	3.1(12)	0.41(12)	M1	3280.9	$10^- \rightarrow 9^-$
	246.4	12(3)	0.30(9)	M1	5576.4	$17^- \rightarrow 16^-$
	308.6	88(16)	0.47(9)	M1	4047.6	$13^- \rightarrow 12^-$
	310.2[a]	–	–	M1	5886.6	$18^- \rightarrow 17^-$
	316.5	16(4)	0.53(13)	M1	4899.2	$15^- \rightarrow 14^-$
	353.1	4.4(16)	–	M1	4385.0	$14^- \rightarrow 13^-$
	421.1	2.4(8)	0.50(17)	M1	5576.4	$17^- \rightarrow 16^-$
	430.8	21(5)	0.35(9)	M1	5330.0	$16^- \rightarrow 15^-$
	470.7	27(7)	1.08(17)	E2	3508.8	$11^- \rightarrow 9^-$
	490.5	10(2)	0.43(8)	M1	3828.9	$12^- \rightarrow 11^-$
	497.8	311(32)	–	E1	3193.0	$11^- \rightarrow 12^+$
	502.2	250(27)	0.39(5)	M1	5155.3	$16^- \rightarrow 15^-$
	519.7	13(3)	–	–	4551.6	$- \rightarrow 13^-$
	520.4	12(3)	0.62(16)	M1	5173.5	$16^- \rightarrow 15^-$
	523.1	21(5)	1.02(16)	E2	4031.9	$13^- \rightarrow 11^-$
	531.6	4.3(9)	–	M1	4653.1	$15^- \rightarrow 15^-$
	535.1	31(6)	0.36(9)	M1	4582.7	$14^- \rightarrow 13^-$
	546.0	190(22)	0.38(7)	M1	3739.0	$12^- \rightarrow 11^-$
	547.8	390(51)	–	E1	3193.0	$11 \rightarrow 10^+$
	548.0	49(9)	1.00(11)	E2	3828.9	$12^- \rightarrow 10^-$

Table 1 (*continued*)

Energy E_γ (keV)	Intensity I_γ (rel.)	R_{DCO}	Multipolarity	Excitation E_i (keV)	Assignment $I_i^\pi \to I_f^\pi$
556.1	32(6)	1.01(11)	E2	4385.0	$14^- \to 12^-$
601.7	13(3)	1.05(16)	E2	4430.6	$14^- \to 12^-$
605.5	259(29)	1.00	E2	4653.1	$15^- \to 13^-$
612.3	5.4(17)	–	M1	5173.5	$16^- \to 15^-$
621.2	13(3)	0.84(19)	E2	4653.1	$15^- \to 13^-$
664.2	12(3)	0.94(21)	E2	4696.1	$15^- \to 13^-$
674.3	4.1(14)	–	M1	5886.6	$18^- \to 17^-$
676.9	3.8(13)	–	M1	5330.0	$16^- \to 15^-$
693.5	45(8)	0.89(14)	E2	4031.9	$13^- \to 11^-$
724.7	5.8(14)	–	E2	5155.3	$16^- \to 14^-$
770.3	5.6(12)	1.08(15)	E2	5155.3	$16^- \to 14^-$
788.5	9.8(25)	0.82(22)	E2	5173.5	$16^- \to 14^-$
851.6	33(9)	1.16(22)	E2	4899.2	$15^- \to 13^-$
854.6	260(31)	1.00	E2	4047.6	$13^- \to 11^-$
868.5	36(9)	0.98(15)	E2	3038.1	$9^- \to 7^-$
873.3	7.8(22)	0.86(18)	E2	3042.9	$9^- \to 7^-$
938.4	9.3(26)	0.94(24)	E2	4986.0	$15^- \to 13^-$
946.9	51(9)	1.04(12)	E2	3280.9	$10^- \to 8^-$
973.1	50(9)	0.85(9)	M1	3280.9	$10^- \to 9^-$
1030.6	72(11)	1.09(12)	E2	3338.4	$11^- \to 9^-$

[a] Very weak transition unresolved from a stronger transition, intensity and DCO ratio could not be determined.
[b] Determination of intensity and DCO ratio is possible only for the doublet.
[c] Determination of DCO ratio is possible only for the doublet.
[d] Determination of intensity is possible only for the multiplet.

lower-lying states. Its decay is fragmented and we observe only a fraction of the intensity in the decay via a few transitions. Four of these transitions, with energies of 142.9, 146.1, 662.3 and 776.8 keV, link the band to the 16^+ levels at 4852.5, 4849.3, 4333.1 and 4218.6 keV, respectively. Two more transitions, with energies of 538.8 and 523.6 keV decay from higher-spin states of band 1 to the 18^+ and 20^+ states of group 1 at 4963.8 and 5708.9 keV, respectively. The DCO ratios of these transitions are compatible with stretched dipoles and the linear polarization of the 662.3 keV transition is negative. Therefore, we assign spin–parity 17^+ to the lowest level of band 1 at 4995.4 keV. A large fraction of the intensity of band 1 decays also to states of group 2. In particular, the 12^+ and 13^- levels at 4589.7 and 4625.8 keV are strongly fed by cascades that include the new low-energy transition of 97 keV and two or three transitions with energies between 100 and 104 keV, but on the basis of the present data it was not possible to establish that decay.

Band 1 and the new band 5 both decay into the 14^+, 15^+ and 16^+ states at 4658.2, 4748.2 and 4852.5 keV, respectively. We assign the transitions of 90.0 and 104.3 keV between these levels to band 5. At high spins we extend band 1 by five transitions up to spin 36^+ and an excitation energy of 12585.5 keV. In addition, we have placed eleven new $\Delta I = 2$ E2 crossover transitions with energies between 449.2 and 1145.7 keV into the level scheme. These transitions, together with the γ-ray intensities, uniquely establish the ordering of the energy levels.

Table 2
Asymmetry ratio A, linear polarization P and adopted multipolarity of some of the transitions of ^{196}Pb

E_γ (keV)	$I_i^\pi \to I_f^\pi$	R_{DCO}	A	P	Multipolarity
Band 1					
192.7	$18^+ \to 17^+$	0.44(5)	−0.116(9)	−0.48(7)	M1
314.5	$19^+ \to 18^+$	0.45(4)	−0.077(6)	−0.35(5)	M1
Decay of band 1					
662.3	$17^+ \to 16^+$	0.45(10)	−0.022(10)	−0.14(6)	M1
Band 2					
203.9	$20^- \to 19^-$	0.47(5)	−0.098(19)	−0.40(9)	M1
267.8	$21^- \to 20^-$	0.50(4)	−0.078(7)	−0.34(5)	M1
Decay of band 2					
582.9	$17^- \to 15^-$	0.90(17)	0.095(22)	0.56(14)	E2
Decay of band 3					
842.4	$20^- \to 18^-$	0.87(20)	0.077(19)	0.58(15)	E2
Decay of band 4					
572.4	$20^+ \to 19^+$	0.38(8)	−0.038(14)	−0.22(9)	M1
Decay of band 5					
702.1	$17^+ \to 16^+$	0.44(9)	−0.043(10)	−0.28(6)	M1
Band 6					
176.2	$15^- \to 14^-$	0.46(9)	−0.054(15)	−0.22(7)	M1
303.2	$16^- \to 15^-$	0.44(8)	−0.056(11)	−0.25(6)	M1
Decay of band 9					
612.3	$16^- \to 15^-$	0.48(9)	−0.039(13)	−0.26(9)	M1
Group 1					
679.2	$16^+ \to 14^+$	1.00	0.091(7)	0.59(10)	E2
Group 2					
421.2	$8^- \to 7^-$	0.61(11)	−0.062(20)	−0.32(11)	M1
803.1	$10^- \to 8^-$	0.94(14)	0.059(19)	0.43(14)	E2
875.0	$12^- \to 11^-$	0.57(11)	−0.013(7)	−0.10(5)	M1
1396.7	$12^+ \to 11^-$	0.55(8)	0.038(10)	0.42(7)	E1
1930.6	$13^- \to 12^-$	0.38(9)	0.017(5)	0.24(7)	E1
Group 3					
467.6	$15^- \to 14^+$	0.60(7)	0.038(4)	0.20(4)	E1
958.7	$14^+ \to 12^+$	1.00	0.064(6)	0.53(7)	E2
Group 4					
164.4	$8^- \to 7^-$	0.55(7)	−0.097(35)	−0.39(15)	M1
502.2	$16^- \to 15^-$	0.39(5)	−0.028(4)	−0.16(3)	M1
548.0	$12^- \to 10^-$	1.00(11)	0.062(18)	0.36(11)	E2
556.1	$14^- \to 12^-$	1.01(11)	0.063(23)	0.37(13)	E2
605.5	$15^- \to 13^-$	1.00	0.097(6)	0.56(7)	E2
851.6	$15^- \to 13^-$	1.16(22)	0.045(18)	0.33(13)	E2
854.6	$13^- \to 11^-$	1.00	0.060(5)	0.46(6)	E2
868.5	$9^- \to 7^-$	0.98(15)	0.064(25)	0.49(19)	E2
946.9	$10^- \to 8^-$	1.04(12)	0.072(13)	0.58(12)	E2
973.1	$10^- \to 9^-$	0.85(9)	−0.040(8)	−0.33(7)	M1
1030.6	$11^- \to 9^-$	1.09(12)	0.077(14)	0.66(13)	E2

3.2. Band 2

In the previous studies [7–9], only band 2 was connected to the lower-lying levels and thus, a spin of $I = 16$ has been assigned to the band head. It decays predominantly via the 502.2 keV transitions to the 15^- state at 4653.1 keV. This transition has a DCO ratio typical for a stretched dipole and its linear polarization is negative, proving its magnetic character. Figure 2 shows a summed coincidence spectrum and a linear polarization spectrum for band 2. Furthermore, the DCO ratios and linear polarizations of the transitions in the cascade down to the previously known [16] 11^- isomer have been determined. The results are compatible with negative parity of the levels involved in the decay of band 2.

An additional low-energy transition of 80.7 keV has been placed above the 5155.3 keV level. It is probably the lowest transition of band 2. However, its intensity and DCO ratio could not be determined since it lies in the region of the X-rays. The placement of this transition is confirmed by the presence of the 582.9 keV E2 crossover transition. In the higher-spin part of band 2 we have reordered some of the M1 transitions on the basis of

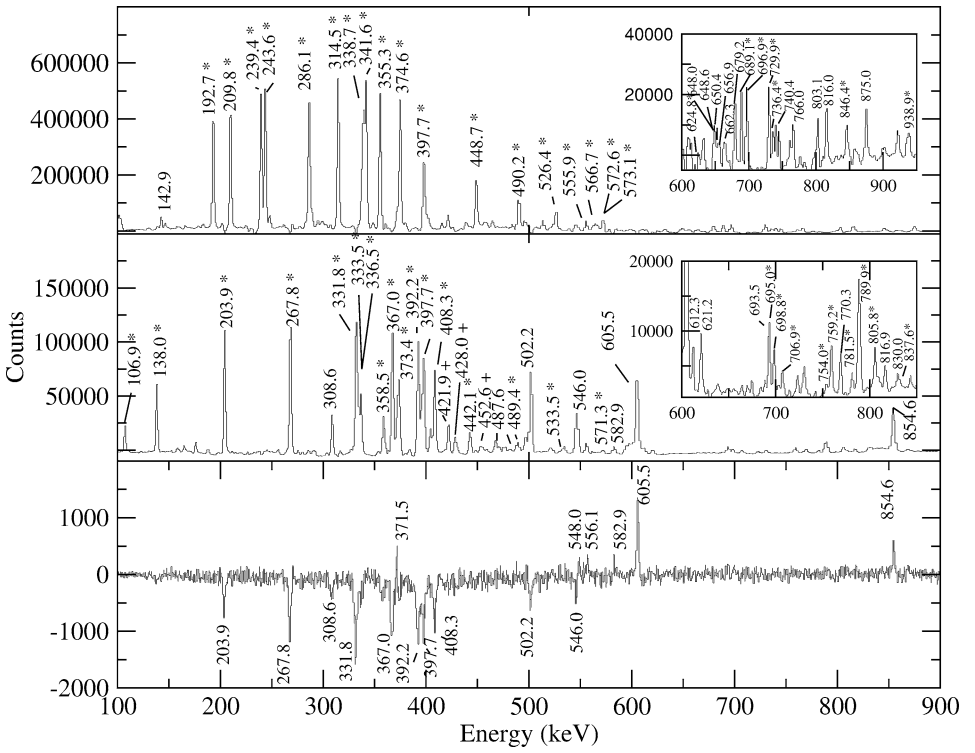

Fig. 2. Summed double gated γ-ray coincidence spectra of band 1 (upper panel) and of band 2 (middle panel). Gates were set on all the transitions of band 1 and on the 106.9, 138.0, 203.9, 267.8, 331.8, 367.0, 392.2, 397.7 and 408.3 keV transitions of band 2. The transitions within the bands are marked by asterisks (*) and those of band 3 which are in coincidence with the transitions of the band 2 mentioned above are marked by plus signs (+). The lower panel shows the linear polarization spectrum for band 2 (see text for details). The gates have been set on the 203.9, 267.8, 331.8, 367.0, 392.2, 397.7 and 408.3 keV transitions.

their intensities and the existence of the E2 crossover transitions. At the highest spins five new transitions have been added, extending the band up to the 36^- state at 12282.6 keV.

3.3. Bands 3 and 3a

Six transitions with energies between 164 and 404 keV were assigned as band 3 in the previous work [7]. We extend this sequence to lower and higher spins and connect it to the lower-lying states of group 4 (see Fig. 1). Furthermore, it decays to low-spin states of band 2 and is also fed from band 2 at higher spins. Band 3 forks above the 25^- state which is fed by a new sequence of three transitions which we label band 3a. Four previously reported M1 transitions between 395 and 428 keV [7] have been incorporated into the high-spin part of band 3. The new ordering of these transitions is uniquely established by its decay into band 2 as well as by two E2 crossover transitions. Band 3 is extended up to the 33^- state at 10956.2 keV. Figure 3 displays two coincidence spectra, one showing the coincidence with the high-spin transitions of band 2 and the other one proving the coincidence with the new sequence above the 25^- state (see Fig. 1).

The strongest transitions in the decay of band 3 are the ones of 842.4 and 851.6 keV for which the DCO and linear polarization results establish E2 multipolarity. The spin–parity assignment is further supported by its decay to band 2 at high spins, in particular, by the fact that the 816.9 and 830.0 keV transitions are compatible with stretched E2 multipolarity.

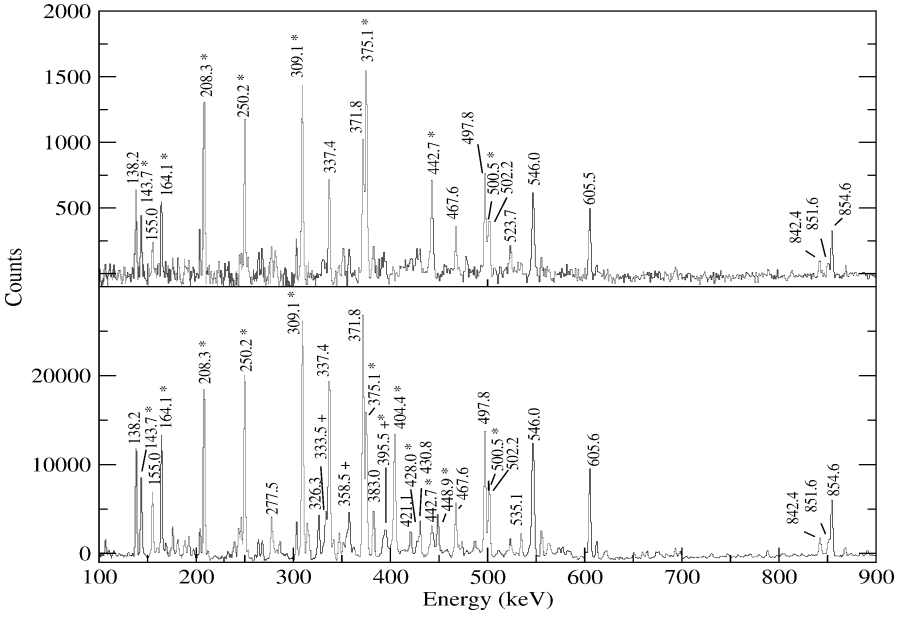

Fig. 3. Summed double gated γ-ray coincidence spectra connected with band 3; the transitions belonging to the band are marked by asterisks (*). The lower spectrum was obtained with gates set on the 143.7, 164.1, 208.3, 250.2, 309.1, 375.1 and 404.4 keV transitions to emphasize its connection to band 2. The transitions belonging to band 2 are marked by plus signs (+). The upper panel shows the summed coincidence spectrum between the 448.9 keV transition and all the γ-ray transitions of band 3.

Thus, we assign spin–parity 18^- and 19^- to the levels at 5886.6 and 6041.6 keV, respectively, both of which may be the band head of band 3.

3.4. Band 4

A few transitions of band 4 have been reported by Moore et al. [8]. In the present work, we firmly establish this band and reorder some of its transitions. It decays into the lower part of band 1. From the decay pattern we assign the spins to band 4 as shown in Fig. 1. Positive parity is assigned to the 20^+ state at 6075.0 keV since the DCO and linear polarization results (see Tables 1 and 2) show that the 572.4 keV transition has M1 multipolarity. Furthermore, the 809.3 and 903.0 keV transitions connecting band 4 with band 1 have DCO ratios compatible with stretched quadrupoles, most likely E2. Figure 4 displays two coincidence spectra which show the decay of band 4 and its coincidence with the new band 8, respectively.

The band head could be either one of the 21^+ states at 6534.1 and 6580.7 keV or the 22^+ level at 6780.1 keV. Band 4 is extended up to the 34^+ state at 11585.6 keV.

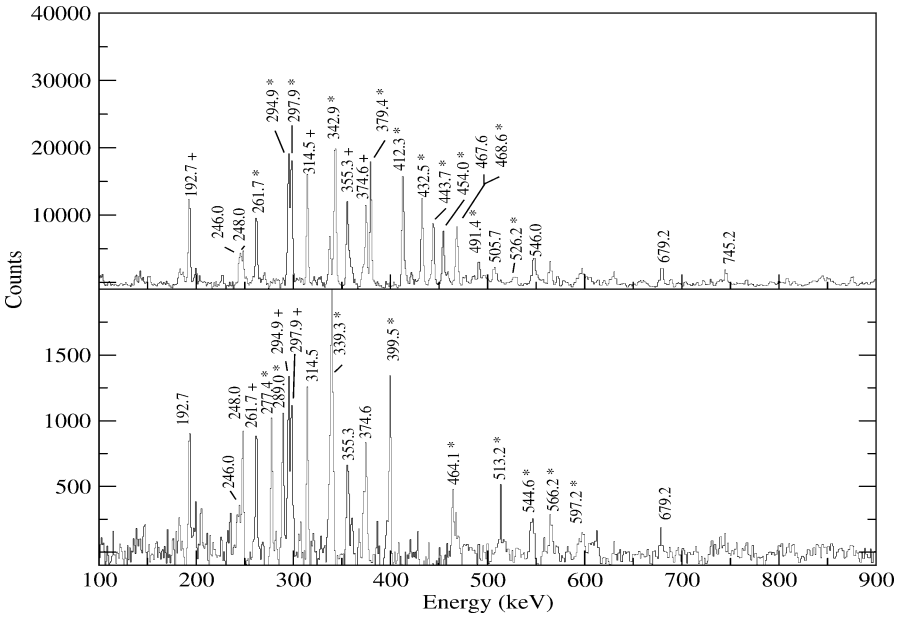

Fig. 4. Summed γ-ray coincidence spectra connected with band 4. Double gates have been set on all the transitions of the band to highlight its decay into band 1 (upper panel). The γ-ray transitions of band 4 are marked by asterisks (*), whereas those of band 1 are marked by plus signs (+). The lower panel shows the summed coincidence spectrum obtained by setting triple gates between the 261.7, 294.9, 297.9 keV transitions of band 4 and the 277.4, 289.0 keV transitions of band 8 to emphasize the coincidences between both bands. In-band transitions of band 8 and band 4 are marked by asterisks (*) and plus (+), respectively.

3.5. New bands 5 to 9

The bands observed for the first time in this work are weakly populated, compare the relative intensities given in Table 1. An exception is band 5 which has an intensity similar to that of band 3. The labeling of the bands given in the level scheme, Fig. 1, is based on their intensities. Band 5 decays to states of group 1, similar to band 1. Since a large fraction of its intensity flows through the 104.3 and 90.0 keV transitions into the 14^+ level at 4658.2 keV, we assign this state as the band head of band 5. A coincidence spectrum connected with band 5 is shown in Fig. 5.

Spins and parities of band 5 are assigned on the basis of the DCO and linear polarization results. In particular, the 702.1 keV connecting transition has M1 and the following 679.2 keV transition has E2 multipolarity (see Tables 1 and 2). Band 5 appears to be rather irregular, but the ordering of the transitions in the band is unambiguously determined by the presence of the E2 crossover transitions.

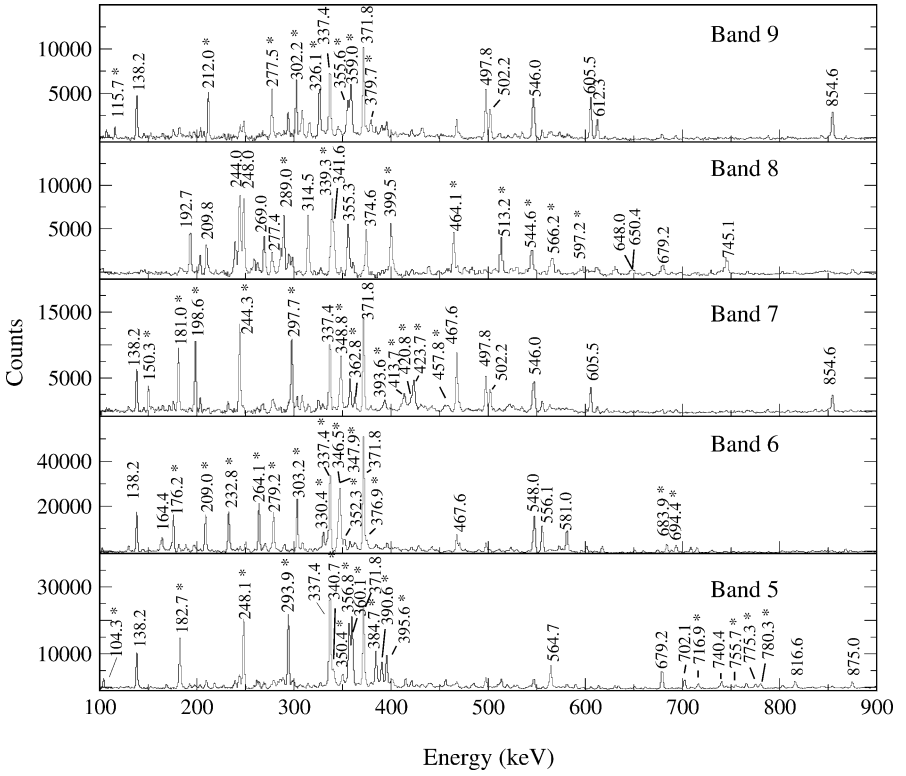

Fig. 5. Summed coincidence spectra for the bands observed for the first time in this work. In-band transitions are marked by asterisks (*). Double gates have been set on the 182.7, 248.1, 293.9 356.8, 360.1 and 395.6 keV transitions of band 5; the 176.2, 209.0, 232.8, 264.1, 279.2, 303.2, 330.4, 347.9 and 352.3 keV transitions of band 6; the 150.3, 181.0, 198.6, 244.3, 297.7, 348.8, 423.7 and 413.7 keV transitions of band 7; the 289.0, 339.3, 399.5, 464.1, 513.2, 544.6 and 566.2 keV transitions of band 8; the 212.0, 277.5, 302.2, 326.1, 355.6 and 359.0 keV transitions of band 9.

Band 6 is irregular in the lower-spin region, but becomes more regular above the 20^- level at 6160.3 keV. It decays into states of group 4 and is connected with band 3 by the 189.1 keV transition from the 21^- state of that band at 6349.4 keV to the 20^- level of band 6. This decay pattern uniquely establishes the spin assignments shown in Fig. 1 and linear polarization results of the cascade down to the 7^- level determine negative parity. A coincidence spectrum connected with band 6 is included in Fig. 5.

Band 7, a rather regular sequence of M1 transitions, is the only one that could not be linked to lower-lying states. Hence, it is not possible to determine spins, parity and excitation energy of this band. It decays predominantly to the 15^- and 16^- levels of group 4 at 4653.1 and 5155.3 keV, respectively. Therefore, we may assume that the band-head spin is 17 or higher. A coincidence spectrum for this band is included in Fig. 5.

Band 8 decays into band 4 via the 277.4 keV stretched dipole transition and into band 1 by five weak transitions for which the DCO ratios could not be determined. These inter-band transitions firmly place band 8 into the level scheme, see Fig. 1. As we could not measure the linear polarization of the inter-band transitions, the parity of this band remains undetermined. The major part of the decay of band 8 could not be established. We observe the transitions of 202.8, 244.0, 247.9, 258.6 and 269.2 keV in coincidence with this band through which most of the intensity is passing to lower-lying states, but they could not be placed uniquely into the level scheme.

The rather irregular sequence which we call band 9 consists of eight transitions. It is mainly decaying through the 612.3 keV magnetic dipole transition to the 15^- level at 4653.1 keV; see the DCO ratio and linear polarization given in Tables 1 and 2. Therefore, we assign spins and parity 16^- through 24^- to the band. In Fig. 5 a coincidence spectrum for band 9 is included.

4. Discussion

4.1. Magnetic rotation

Magnetic rotation occurs in near-spherical nuclei when the symmetry is broken by anisotropic current distributions of a few excited nucleons with large angular momenta. It manifests itself in rotational-like bands with strong $\Delta I = 1$ M1 transitions and very weak $\Delta I = 2$ E2 crossover transitions. In the Pb region the MR bands are built on high-spin proton–particle excitations ($\pi h_{9/2}$ and $\pi i_{13/2}$) coupled to high-spin neutron–hole states ($\nu i_{13/2}^{-n}$) [12,17]. Such proton excitations into the $h_{9/2}$ and/or $i_{13/2}$ levels above the $Z = 82$ shell gap, e.g., the $\pi(h_{9/2}^2)8^+$ or $\pi(h_{9/2}\ i_{13/2})11^-$ states, are known in the Pb and Po isotopes [1]. They are slightly oblate deformed [18]. However, no rotational bands built directly on these states are observed. Similarly, high-spin neutron–hole states, e.g., the $\nu(i_{13/2}^{-2})12^+$ and $\nu(i_{13/2}^{-3})33/2^+$ states, occur in the Pb isotopes without the observation of rotational bands built on these excitations [1]. The M1 bands occur only when the high-spin proton excitations are coupled to the high-spin neutron–hole states.

The particle–hole coupling favors a near perpendicular orientation of the proton–particle and neutron–hole spins. This coupling has been verified for the band head of a MR band in

^{193}Pb by a g-factor measurement [17]. With increasing spin, within the bands, the proton and neutron spins align step-by-step into the direction of the total angular momentum. Since this resembles the closing of the blades of a pair of shears, the MR bands have previously been called 'shears bands' [19]. As a consequence of the shears mechanism the total angular momentum, that points somewhere between the proton and neutron spins and does not coincide with one of the principal axes of the slightly oblate-deformed nucleus, remains almost constant in direction in the intrinsic system. The shears effect has been tested by lifetime measurements [20–24]. It was shown that the reduced transition probabilities for the M1 transitions within the bands decrease with increasing spin. This is expected, since the $B(\mathrm{M1})$ values depend on the perpendicular component of the magnetic moment which decreases when the protons and neutrons align along the total-spin direction [22,24].

The $B(\mathrm{M1})/B(\mathrm{E2})$ ratios derived from the present data are summarized in Table 3. These ratios are very large, much larger than those observed in deformed nuclei. This is expected for magnetic rotation where the $B(\mathrm{M1})$ values are large, due to the large magnetic moment component perpendicular to the total angular momentum, and the $B(\mathrm{E2})$ values are small, due to the small quadrupole deformation. Combined with the recent lifetime measurements for band 1 in ^{196}Pb [20,22] these results give $B(\mathrm{E2})$ values around 0.1–0.3 $e^2\,\mathrm{b}^2$. Unfortunately the uncertainties are large, typically 30 to 50%, because of the very low intensities of the E2 crossover transitions. Nevertheless, the deformation parameters $|\beta_2|$ derived from these $B(\mathrm{E2})$ values are typically below 0.1.

Calculations within the framework of the TAC model [4,5,10,19] have been performed for the MR bands in ^{196}Pb. Compared to our previous calculations [19], we have made the following changes [25]:

(i) The TAC quadrupole–quadrupole coupling constant was adjusted to reproduce the experimental quadrupole moment of the 12^+ isomer in ^{196}Pb [26]; and
(ii) the deformation within the bands was calculated self-consistently.

We adopt the nomenclature introduced in Ref. [19] to classify the bands. For the neutrons, pairing is taken into account in the calculations because the Fermi level lies well below the $N = 126$ shell closure. Therefore, the neutron configurations are labeled by the letters A, B, C and D for quasineutrons of $i_{13/2}$ origin and E, F, G, ... for the natural-parity quasineutrons (mainly of $p_{3/2}, f_{5/2}$ origin), as in the standard cranked shell model. The proton pairing is neglected because we are dealing only with two protons outside the closed $Z = 82$ shell. Therefore, the proton configuration can be abbreviated by its spin quantum number. For example, the configuration with two quasineutrons of $\nu i_{13/2}$ origin coupled to the proton $\pi(h^2_{9/2})8^+$ excitation is labeled AB8 [19].

The shears mechanism has been investigated in terms of an effective interaction between the proton and neutron 'blades' by Macchiavelli et al. [3,27–30]. These authors have shown that the rotational-like bands can be well reproduced with an interaction of the type $V_2 P_2(\cos\theta)$, where θ is the angle between the proton and neutron spins. For the particle–hole coupling in the case of the shears bands the interaction strength V_2 is positive, resulting in a minimum of the interaction energy at $\theta = 90°$, which is the situation at the band head. An analysis of the interaction strength for many bands in the Pb isotopes [12,

Table 3
$B(\mathrm{M1})/B(\mathrm{E2})$ ratios for some of the bands in ^{196}Pb calculated from γ-ray intensities

E_γ^{M1} (keV)	$I_i^\pi \to I_f^\pi$	E_γ^{E2} (keV)	$I_i^\pi \to I_f^\pi$	$B(\mathrm{M1})/B(\mathrm{E2})$ ($\mu_N^2/(e\,\mathrm{b})^2$)
Band 1				
314.5	$19^+ \to 18^+$	507.2	$19^+ \to 17^+$	16(4)
374.6	$20^+ \to 19^+$	689.1	$20^+ \to 18^+$	19(4)
355.3	$21^+ \to 20^+$	729.9	$21^+ \to 19^+$	21(4)
341.6	$22^+ \to 21^+$	696.9	$22^+ \to 20^+$	19(5)
243.6	$23^+ \to 22^+$	585.2	$23^+ \to 21^+$	47(12)
209.8	$24^+ \to 23^+$	453.4	$24^+ \to 22^+$	42(13)
338.7	$27^+ \to 26^+$	624.8	$27^+ \to 25^+$	25(7)
397.7	$28^+ \to 27^+$	736.4	$28^+ \to 26^+$	19(5)
448.7	$29^+ \to 28^+$	846.4	$29^+ \to 27^+$	17(5)
490.2	$30^+ \to 29^+$	938.9	$30^+ \to 28^+$	21(7)
526.4	$31^+ \to 30^+$	1016.6	$31^+ \to 29^+$	23(8)
555.9	$32^+ \to 31^+$	1082.3	$32^+ \to 30^+$	16(8)
Band 2				
267.8	$21^- \to 20^-$	471.7	$21^- \to 19^-$	24(6)
331.8	$22^- \to 21^-$	599.6	$22^- \to 20^-$	33(9)
367.0	$23^- \to 22^-$	698.8	$23^- \to 21^-$	20(5)
392.2	$24^- \to 23^-$	759.2	$24^- \to 22^-$	19(5)
397.7	$25^- \to 24^-$	789.9	$25^- \to 23^-$	17(4)
408.3	$26^- \to 25^-$	805.8	$26^- \to 24^-$	15(4)
373.4	$27^- \to 26^-$	781.5	$27^- \to 25^-$	29(8)
333.5	$28^- \to 27^-$	706.9	$28^- \to 26^-$	38(9)
336.5	$29^- \to 28^-$	670.0	$29^- \to 27^-$	27(10)
358.5	$30^- \to 29^-$	695.0	$30^- \to 28^-$	16(5)
395.5	$31^- \to 30^-$	754.0	$31^- \to 29^-$	14(5)
442.1	$32^- \to 31^-$	837.6	$32^- \to 30^-$	11(4)
Band 3				
404.1	$29^- \to 28^-$	799.1	$29^- \to 27^-$	19(5)
452.6	$31^- \to 30^-$	880.6	$31^- \to 29^-$	14(5)
Band 5				
293.9	$19^+ \to 18^+$	542.0	$19^+ \to 17^+$	15(4)
356.8	$20^+ \to 19^+$	650.7	$20^+ \to 18^+$	13(3)
360.1	$21^+ \to 20^+$	716.9	$21^+ \to 19^+$	< 16
395.6	$22^+ \to 21^+$	755.7	$22^+ \to 20^+$	17(5)
384.7	$23^+ \to 22^+$	780.3	$23^+ \to 21^+$	16(5)
390.6	$24^+ \to 23^+$	775.3	$24^+ \to 22^+$	14(5)
Band 6				
347.9	$17^- \to 16^-$	651.1	$17^- \to 15^-$	12(4)
346.5	$18^- \to 17^-$	694.4	$18^- \to 16^-$	14(4)
337.4	$19^- \to 18^-$	683.9	$19^- \to 17^-$	9(3)

28] resulted in an average V_2 of 2.3 MeV which corresponds to 400–600 keV per proton–neutron pair. It has been argued [28,29] that the particle-vibration coupling can give rise to a P_2-type interaction with a comparable strength.

4.2. Positive-parity bands

Configuration assignments have been made previously only to bands 1 and 2 [7–9, 20,22]. Band 1, for which we establish positive parity, is the most strongly populated band in ^{196}Pb. Its band head is probably the 17^+ level at 4995.4 keV. The 14^+ state at 4658.2 keV, and the 15^+ and 16^+ levels above it, are mainly populated by band 5, see Fig. 1. Thus we have assigned the 14^+ level to band 5, but on the basis of the present data it cannot be decided with certainty to which of the two bands these three levels belong. Despite this uncertainty, band 1 starts at low spin and has a low excitation energy, as can be seen in the upper panel of Fig. 6 where the excitation energies of the positive-parity bands in ^{196}Pb are plotted as a function of spin.

The excitation energies calculated within the framework of the TAC model have been normalized to the 18^- state in band 2 because its configuration contains the two-quasineutron excitation that has been used to adjust the quadrupole-quadrupole coupling constant [25]. For the positive-parity bands these energies are plotted in the lower panel of Fig. 6. Three configurations have low excitation energies and start at low spin, the AB8, AE11 and AF11 configurations. In the previous work [7–9], the configuration AE11 was suggested for band 1. We concur with this suggestion. Support for this assignment comes from the systematic behavior of these bands in ^{194,196,198}Pb [12]. They all show the first band crossing at a rotational frequency of about 0.29 MeV. At this frequency a pair of $i_{13/2}$ neutrons (BC) decouples and aligns with an alignment gain of $7.5\hbar$. Thus, the AE11 configuration is crossed by the ABCE11 configuration.

The spin of the positive-parity bands in ^{196}Pb is plotted as a function of the frequency in the upper panel of Fig. 7. As can be seen, for band 1 the first crossing occurs at a frequency

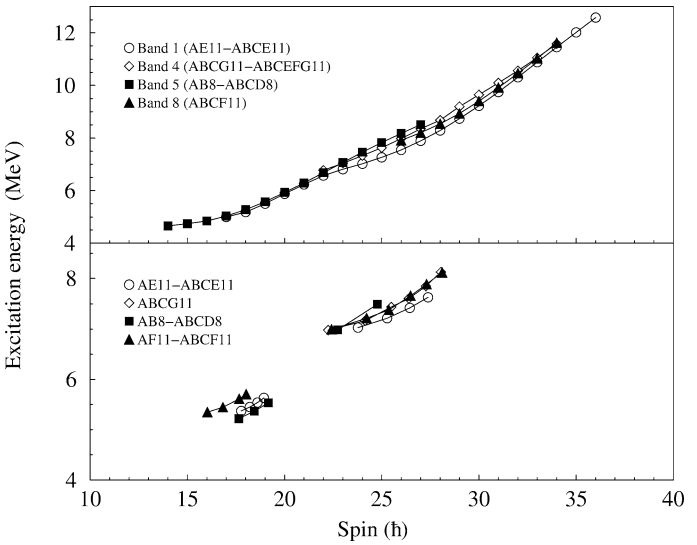

Fig. 6. Experimental (upper panel) and calculated (lower panel) excitation energies as a function of spin for the positive-parity bands in ^{196}Pb.

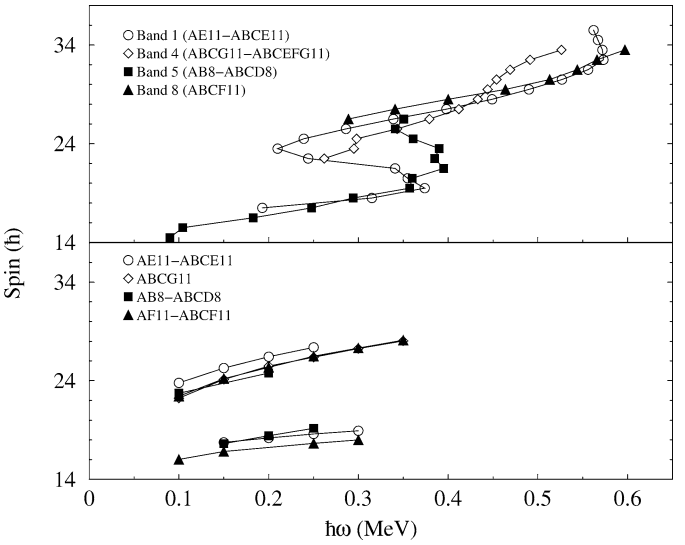

Fig. 7. Experimental (upper panel) and calculated (lower panel) spins as a function of rotational frequency, $\hbar\omega = E_\gamma$, for the positive-parity bands in ^{196}Pb.

of 0.29 MeV, which is typical for the BC alignment in the MR bands in the Pb isotopes [12]. Thus, the configuration AB8 is ruled out, since here the BC alignment is blocked. The gain in alignment of band 1 at the first crossing is $7.4\hbar$, in agreement with the calculation shown in the lower panel of Fig. 7.

As seen in Fig. 7, at the highest observed frequencies, above $\hbar\omega = 0.55$ MeV, band 1 shows another gain in alignment. This occurs in the spin range where the ABCE11 configuration has exhausted its spin, i.e., when all the spins of the valence nucleons are aligned (including a small contribution from other low-spin particles, which may be called a 'core' contribution). Thus, the ABCE11 band terminates around spin 32 and, possibly, a new configuration with an additional pair of aligned nucleons sets in. Judging from the observed onset of the backbending, the gain in alignment seems to be at least $4\hbar$. The alignment of the next pair of $i_{13/2}$ neutrons could contribute up to $6\hbar$. An alternative would be the alignment of a pair of $h_{11/2}$ protons which would give rise to a higher alignment gain. Such a proton alignment has been suggested to explain the M1 structures observed at high spin in the Hg isotopes [31–35]. It has recently been speculated that the proton $h_{11/2}$ alignment might play a role also in the structure of M1 bands in ^{194}Pb [36]. However, without the knowledge of the full alignment gain it is difficult to decide about its origin.

Kemper et al. [20] have measured lifetimes in the lower part of band 1. The B(M1) values derived from these data were compared to calculations using the semiclassical model suggested by Macchiavelli et al. [27,28,30]. This comparison slightly favors the AF11 configuration for the lower part of band 1 over the AE11 configuration. Our TAC calculations also give similar B(M1) values for the AE11 and AF11 configurations. Given the large uncertainties of the experimental B(M1) values [20,22], the comparison with the theory cannot distinguish between these two possibilities.

Before turning to the negative-parity bands, we want to discuss the possible configurations of the remaining positive-parity bands. Band 4 decays into states of band 1 below the band crossing. Thus, the two bands may have similar configurations. As it lies higher in excitation energy but has lower spin in its lower-frequency region than both band 1 and band 8 with the ABCE11 and ABCF11 (see below) configurations, respectively, the configuration of band 4 might be ABCG11. At a frequency around 0.45 MeV it shows a gain in alignment which is not seen in bands 1 and 8, see Fig. 7. It may be speculated that another pair of natural-parity neutrons (EF) aligns at that frequency.

In ^{194}Pb a short sequence of M1 transitions (named band 2c) has been observed [36] which shows a similar decay pattern as band 4 in ^{196}Pb: it also decays into the AE11 band. It was speculated [36] that an aligned $h_{11/2}$ proton pair is coupled to the AE11 configuration. Such a two-neutron/four-proton structure can account for the band-head spin. However, it would result in smaller B(M1) values which would make it difficult to explain why we do not observe competing E2 crossover transitions in band 4. In fact, our preliminary analysis of lifetimes of states in band 4 shows that the B(M1) values are similar to those of the other bands. Furthermore, it could not be understood why the alignment of the next $i_{13/2}$ neutron pair (BC) with its large alignment gain should not be observed in such a band.

The new band 5 extends down to even lower spin as band 1 and has also low excitation energy. Comparison to the results of the TAC calculations suggests that it may be a candidate for the configuration AB8. Another possibility is the configuration AF11. However, as can be seen in Fig. 7, band 5 does not show the BC crossing which is seen in band 1 and would be expected for the AF11 configuration. Therefore, we favor the AB8 assignment for band 5. A similar band has recently been observed [36] in ^{194}Pb and has also been assigned the AB8 configuration. Above spin 20 band 5 becomes irregular with six transitions of rather similar energy. This spin is around the maximum that can be expected for the AB8 configuration, with all the valence nucleons aligned and a small 'core' contribution. The systematics of the band crossings shows [12] that the MR bands with four aligned $\nu i_{13/2}$ neutron holes (ABCD) start at rotational frequencies around 0.35 MeV. Thus, it seems likely that we are observing the onset of the ABCD8 band. Due to its low intensity, we do not observe band 5 up to sufficiently high spins to see this new band.

Band 8, also with positive parity, is a candidate for the ABCF11 configuration. It lies slightly higher in excitation energy than the ABCE11 configuration in the high-spin part of band 1, see upper panel of Fig. 6. Furthermore, it decays via a series of dipole, presumably M1, transitions into band 1 with the ABCE11 configuration, see the level scheme in Fig. 1. Such a decay pattern has been observed previously between the ABE11 and ABF11 configurations in ^{199}Pb [19].

If band 8 has indeed the ABCF11 configuration, as suggested here, the question arises why we do not observe it to lower spins through the band crossing down to the AF11 configuration. As pointed out in Section 3.5, we do observe several transitions which must lie below the $26^{(+)}$ level of that band. They may be part of the continuation of band 8 to lower spins and, thus, into the AF11 configuration. However, this band is rather week and we are not certain about the ordering of these transitions. Therefore, they are not shown in the level scheme of Fig. 1.

4.3. Negative-parity bands

Let us now turn to the negative-parity bands. Their excitation energies as a function of spin and their spins as a function of rotational frequency are displayed in Figs. 8 and 9, respectively. Although its spins are not uniquely determined, band 7 is also included in the latter figure; we have assumed spin and parity 17^- for the band head. Band 2 was the only band that had previously been connected to lower-lying levels. The AB11 and ABCD11 configurations below and above the band crossing, respectively, have been assigned previously [7–9] to this band. The excitation energy, the alignment behavior (an alignment gain of $7.4\hbar$ at a rotational frequency of 0.37 MeV) and the systematics of similar bands in the neighboring Pb isotopes [12] support this assignment.

Band 3 starts at spin 18 or 19 and at an excitation energy of about 700 keV above band 2 with the AB11 configuration, see Figs. 8 and 9. Therefore, its structure probably involves an additional pair of aligned quasineutrons and we suggest the configuration ABEF11. At spins 26 and 27 band 3 shows an irregularity. This is the spin region where this configuration is expected to terminate. Several inter-band transitions are observed between bands 2 and 3, see level scheme in Fig. 1, and the short new sequence of three levels with spins 26, 27 and 28 (labeled band 3a in Fig. 1) decays into band 3. The 26^- and 27^- states of bands 2, 3 and 3a lie rather close in energy and are probably strongly mixed. This mixing can explain the inter-band transitions. In fact, the 27^- state of band 3 predominantly decays into band 2 via the 421.9 keV transition. However, one has to note that the 375 keV in-band transition is a doublet in band 3. Thus, its intensity cannot be determined accurately and the in-band to out-of-band intensity ratio $I_\gamma(375)/I_\gamma(422)$ has a large uncertainty.

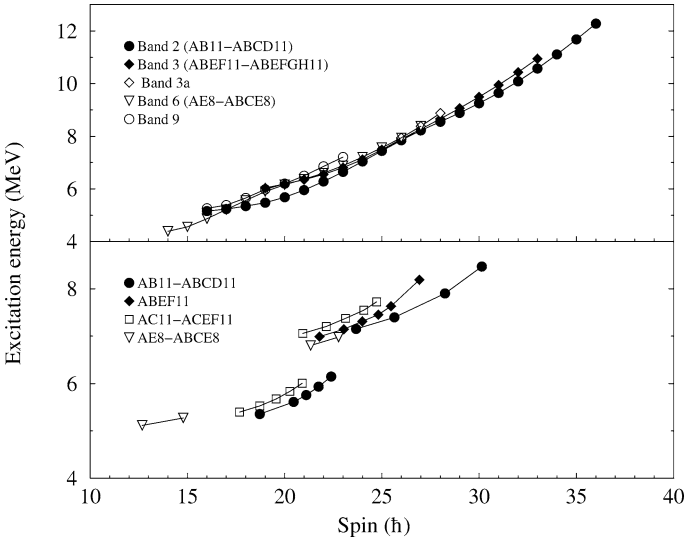

Fig. 8. Experimental (upper panel) and calculated (lower panel) excitation energies as a function of spin for the negative-parity bands in ^{196}Pb.

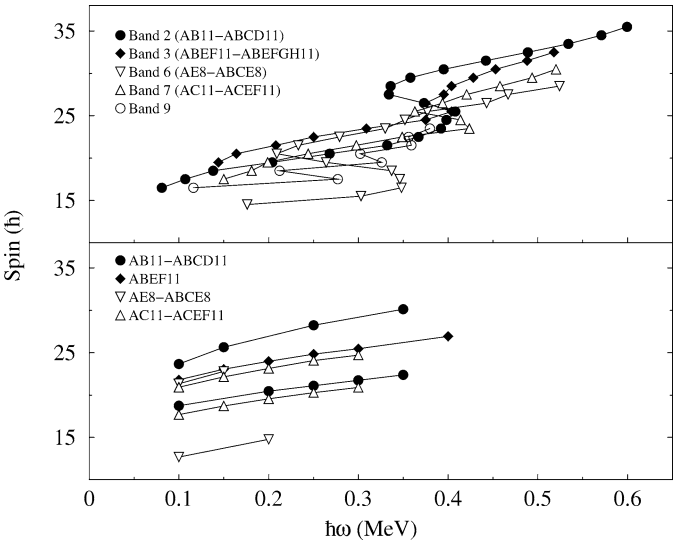

Fig. 9. Experimental (upper panel) and calculated (lower panel) spins as a function of rotational frequency, $\hbar\omega = E_\gamma$, for the negative-parity bands in ^{196}Pb. For the band head of band 8 a spin of $17\hbar$ was assumed in this plot.

The high-spin part of band 3 has a higher alignment than the lower-spin region. The gain in alignment is smaller and occurs at a slightly higher frequency than the CD alignment observed in band 2, see upper panel of Fig. 9. A possible explanation is the alignment of the next pair of natural-parity neutrons (GH), forming the ABEFGH11 configuration. The slope of the alignment curve in the high-spin part of band 3 is different from that of band 2. This may indicate a gradual alignment process, possibly of $i_{13/2}$ quasineutrons mixing into the configuration.

The new band 6 shows a first band crossing around $\hbar\omega = 0.29$ MeV which is typical for the BC crossing. Its band head has low excitation energy and low spin, see Figs. 9 and 10. Comparison to the TAC calculations shows that the simplest and lowest-energy configuration would be AE8 and ABCE8 below and above this crossing, respectively. Evidence for a band which probably has also the ABCE8 configuration has recently been presented [36] for the neighboring isotope ^{194}Pb.

Band 7 is the only MR band in ^{196}Pb that is not connected to lower-lying states. From its decay pattern we tentatively assign spin-parity 17^- to the band head. Under this assumption it has been included in Fig. 9 which shows that it starts with a similar alignment as the AB11 band 2, but with a smaller one than the ABEF11 band 3 and the ABCE8 band 6. At a rotational frequency of 0.4 MeV, which is close to the CD crossing frequency observed for band 2, band 7 shows a gain in alignment of $3.7\hbar$. This is only about half of that of the CD alignment. The TAC calculations give rather similar alignments for the ABEF11, ACEF11 (see lower panel of Fig. 9) and ABEG11 configurations, all of them lying between the AB11 and ABCD11 alignments. The most reasonable assignment for band 7 at high frequencies would be ACEF11, because ABEF11 has already been assigned to band 3 and ABEG11 is unlikely as it would involve a more complicated rearrangement

Table 4
Configuration assignments to magnetic-rotational bands in ^{196}Pb

Band	Configuration		
#	below crossing	above 1st crossing	above 2nd crossing
1	AE11	ABCE11	?
2	AB11	ABCD11	–
3	–	ABEF11	(ABEFGH11)
4	–	(ABCG11)	(ABCEFG11)
5	AB8	ABCD8	–
6	AE8	ABCE8	–
7	(AC11)	(ACEF11)	–
8		(ABCF11)	

in the crossing region. With our suggestion of ACEF11 above the crossing, band 7 could have the AC11 configuration below the crossing. One might expect a somewhat lower band-head spin for the AC11 configuration than that for the AB11 band 2. However, the rotational frequency at which band 7 starts is also higher than that of band 2. This may have caused the 'shears to be slightly closed' near the band head. On the other hand, we have to keep in mind that the spin of band 7 is not firmly established experimentally.

The sequence which we call band 9 is rather irregular and shows a different behavior than the other bands in ^{196}Pb. On the basis of the present information we do not want to speculate on the configuration of this sequence. Due to its irregularity it even may not qualify as a MR band.

The configuration assignments to the bands in ^{196}Pb that could be suggested on the basis of the present data, by comparison to the systematic behavior of the MR bands in the Pb isotopes [12] and by comparison to TAC calculations are summarized in Table 4.

5. Summary

In summary, high-spin states in ^{196}Pb were investigated in two experiments using the EUROBALL γ-ray spectrometer array. Five new MR bands have been found and the previously known four bands have been extended to higher and lower spins and their levels have partly been reordered. All the bands, with one exception, have been connected to lower-lying states and excitation energies, spins and parities have been determined. Using these data and comparing band crossing frequencies and aligned angular momenta to neighboring isotopes as well as to TAC calculations, arguments are made for configuration assignments to all but one of the bands. The MR bands in this mass region to which reliable configuration assignments can be made are explained with either the $(h_{9/2}i_{13/2})11^-$ or the $(h^2_{9/2})8^+$ proton particle state coupled to high-spin quasineutron hole-excitations.

Acknowledgements

We wish to thank the staff of the Legnaro and Strasbourg accelerators for providing the beams and we greatly appreciate the technical support in running the EUROBALL spectrometer at both laboratories. We thank M.G. Porquet and M. Kaci for an early communication of their result on the ^{196}Pb level scheme. One of us, A.K.S., acknowledges a fellowship from the A. von Humboldt foundation. The work was supported by BMBF (Germany) under the contract 06 BN 907 and by DFG (Germany) under contract HU 325/10. Support by the EU under contracts ERBFMBICT961027, ERBFMGECT970123, ERBFMGECT980145 and HPRICT199900079 is gratefully acknowledged.

References

[1] R.B. Firestone, in: V.S. Shirley, C.M. Baglin, S.Y.F. Chu, J. Zipkin (Eds.), Table of Isotopes, Wiley, 1996.
[2] Amita, A.K. Jain, B. Singh, At. Data Nucl. Data Tables 74 (2000) 283.
[3] R.M. Clark, A.O. Macchiavelli, Annu. Rev. Nucl. Part. Sci. 501 (2000) 1.
[4] S. Frauendorf, Z. Phys. A 358 (1997) 163.
[5] S. Frauendorf, Rev. Mod. Phys. 73 (2001) 463.
[6] J. Simpson, Z. Phys. A 358 (1997) 139.
[7] G. Baldsiefen, H. Hübel, W. Korten, U.J. van Severen, J.A. Cizewski, N.H. Medina, D.R. Napoli, C. Rossi Alvarez, G. LoBianco, S. Signorelli, Z. Phys. A 355 (1996) 337.
[8] E.F. Moore, M.P. Carpenter, Y. Liang, R.V.F. Janssens, I. Ahmad, I.G. Bearden, P.J. Daly, M.W. Drigert, B. Fornal, U. Garg, Z.W. Grabowski, H.L. Harrington, R.G. Henry, T.L. Khoo, T. Lauritsen, R.H. Mayer, D. Nisius, W. Reviol, M. Sferrazza, Phys. Rev. C 51 (1995) 115.
[9] J.R. Hughes, Y. Liang, R.V.F. Janssens, A. Kuhnert, J.A. Becker, I. Ahmad, I.G. Bearden, M.J. Brinkman, J. Burde, M.P. Carpenter, J.A. Cizewski, P.J. Daly, M.A. Deleplanque, R.M. Diamond, J.E. Draper, C. Duyar, B. Fornal, U. Garg, Z.W. Grabowski, E.A. Henry, R.G. Henry, W. Hesselink, N. Kalantar-Nayestanaki, W.H. Kelly, T.L. Khoo, T. Lauritsen, R.H. Mayer, D. Nisius, J.R.B. Oliveira, A.J.M. Plompen, W. Reviol, E. Rubel, F. Soramel, F.S. Stephens, M.A. Stoyer, D. Vo, T.F. Wang, Phys. Rev. C 47 (1993) R1337.
[10] S. Frauendorf, Nucl. Phys. A 557 (1993) 259c.
[11] B. Schlitt, U. Maier, H. Friedrichs, S. Albers, I. Bauske, P. von Brentano, R.D. Heil, R.-D. Herzberg, U. Kneissl, J. Margraf, H.H. Pitz, C. Wesselborg, A. Zilges, Nucl. Instrum. Methods Phys. Res. A 337 (1994) 416.
[12] A. Görgen, N. Nenoff, H. Hübel, G. Baldsiefen, J.A. Becker, A.P. Byrne, S. Chmel, R.M. Clark, M.A. Deleplanque, R.M. Diamond, P. Fallon, K. Hauschild, I.M. Hibbert, W. Korten, R. Krücken, I.Y. Lee, A.O. Macchiavelli, E.S. Paul, U.J. van Severen, F.S. Stephens, K. Vetter, R. Wadsworth, A.N. Wilson, J.N. Wilson, Nucl. Phys. A 683 (2001) 108.
[13] O. Klein, Y. Nishina, Z. Phys. 52 (1929) 853.
[14] D. Rossbach, A. Görgen, H. Hübel, E. Mergel, G. Schönwasser, A.N. Wilson, F. Azaiez, A. Astier, D. Bazzacco, M. Bergström, C. Bourgeois, N. Buforn, F. Hannachi, K. Hauschild, A. Korichi, W. Korten, T. Kröll, A. Lopez-Martens, R. Lucas, H.J. Maier, N. Redon, P. Reiter, C. Rossi-Alvarez, O. Stezowski, P. Thirolf, Phys. Lett. B 513 (2001) 9.
[15] J. Penninga, W.H.A. Hesselink, A. Balanda, A. Stolk, H. Verheul, J. van Klinken, H.J. Riezebos, M.J.A. de Voigt, Nucl. Phys. A 471 (1987) 535.
[16] J.J. Van Ruyven, J. Penninga, W.H.A. Hesselink, P. Van Nes, K. Allaart, E.J. Hengveld, H. Verheul, M.J.A. De Voigt, Z. Sujkowski, J. Blomqvist, Nucl. Phys. A 449 (1986) 579.
[17] S. Chmel, F. Brandolini, R.V. Ribas, G. Baldsiefen, A. Görgen, M. De Poli, P. Pavan, H. Hübel, Phys. Rev. Lett. 79 (1997) 2002.
[18] K. Vyvey, S. Chmel, G. Neyens, H. Hübel, D.L. Balabanski, D. Borremans, N. Coulier, R. Coussement, W. De Clercq, G. Georgiev, N. Nenoff, S.C. Pancholi, D. Rossbach, R. Schwengner, S. Teughels, S. Frauendorf, Phys. Rev. Lett., in press.

[19] G. Baldsiefen, H. Hübel, W. Korten, D. Mehta, N. Nenoff, B.V. Thirumala Rao, P. Willsau, H. Grawe, J. Heese, H. Kluge, K.H. Maier, R. Schubart, S. Frauendorf, H.J. Maier, Nucl. Phys. A 574 (1994) 521.
[20] G. Kemper, A. Dewald, I. Wiedenhöver, R. Peusquens, S. Kasemann, K.O. Zell, P. von Brentano, H. Hübel, S. Chmel, A. Görgen, D. Bazzacco, R. Venturelli, S. Lunardi, D.R. Napoli, F. Hannachi, A. Lopez-Martens, R. Krücken, J.R. Cooper, R.M. Clark, M.A. Deleplanque, I.Y. Lee, A.O. Macchiavelli, F.S. Stephens, Eur. Phys. J. A 11 (2001) 121.
[21] R.M. Clark, S.J. Asztalos, G. Baldsiefen, J.A. Becker, L. Bernstein, M.A. Deleplanque, R.M. Diamond, P. Fallon, I.M. Hibbert, H. Hübel, R. Krücken, I.Y. Lee, A.O. Macchiavelli, R.W. MacLeod, G. Schmid, F.S. Stephens, K. Vetter, R. Wadsworth, S. Frauendorf, Phys. Rev. Lett. 78 (1997) 1868.
[22] R.M. Clark, R. Krüken, S.J. Asztalos, J.A. Becker, B. Busse, S. Chmel, M.A. Deleplanque, R.M. Diamond, P. Fallon, D. Jenkins, K. Hauschild, I.M. Hibbert, H. Hübel, I.Y. Lee, A.O. Macchiavelli, R.W. MacLeod, G. Schmid, F.S. Stephens, U.J. van Severen, K. Vetter, R. Wadsworth, S. Wan, Phys. Lett. B 440 (1998) 251.
[23] R. Krücken, R.M. Clark, A. Dewald, M.A. Deleplanque, R.M. Diamond, P. Fallon, K. Hauschild, I.Y. Lee, A.O. Macchiavelli, R. Peusquens, G.J. Schmid, F.S. Stephens, K. Vetter, P. von Brentano, Phys. Rev. C 58 (1998) R1876.
[24] M. Neffgen, G. Baldsiefen, S. Frauendorf, H. Grawe, J. Heese, H. Hübel, H. Kluge, A. Korichi, W. Korten, K.H. Maier, D. Mehta, J. Meng, N. Nenoff, M. Piiparinen, M. Schönhofer, R. Schubart, U.J. van Severen, N. Singh, G. Sletten, B.V. Thirumala Rao, P. Willsau, Nucl. Phys. A 595 (1995) 499.
[25] S. Chmel, H. Hübel, S. Frauendorf, to be published.
[26] S. Zywietz, H. Grawe, H. Haas, M. Menningen, Hyperfine Interact. 9 (1981) 109.
[27] A.O. Macchiavelli, R.M. Clark, P. Fallon, M.A. Deleplanque, R.M. Diamond, R. Krücken, I.Y. Lee, F.S. Stephens, S. Asztalos, K. Vetter, Phys. Rev. C 57 (1998) R1073.
[28] A.O. Macchiavelli, R.M. Clark, M.A. Deleplanque, R.M. Diamond, P. Fallon, I.Y. Lee, F.S. Stephens, K. Vetter, Phys. Rev. C 58 (1998) R621.
[29] A.O. Macchiavelli, R.M. Clark, M.A. Deleplanque, R.M. Diamond, P. Fallon, I.Y. Lee, F.S. Stephens, K. Vetter, Phys. Rev. C 58 (1998) 3746.
[30] A.O. Macchiavelli, R.M. Clark, M.A. Deleplanque, R.M. Diamond, P. Fallon, I.Y. Lee, F.S. Stephens, K. Vetter, Phys. Lett. B 450 (1999) 1.
[31] B. Cederwall, M.A. Deleplanque, F. Azaiez, R.M. Diamond, P. Fallon, W. Korten, I.Y. Lee, A.O. Macchiavelli, J.R.B. Oliveira, F.S. Stephens, W.H. Kelly, D.T. Vo, J.A. Becker, M.J. Brinkman, E.A. Henry, J.R. Hughes, A. Kuhnert, M.A. Stoyer, T.F. Wang, J.E. Draper, C. Duyar, E. Rubel, J. deBoer, Phys. Rev. C 47 (1993) R2443.
[32] Y. LeCoz, N. Redon, A. Astier, R. Béraud, R. Duffait, M. Meyer, F. Hannachi, G. Bastin, I. Deloncle, B. Gall, M. Kaci, M.G. Porquet, C. Schück, F. Azaiez, C. Bourgeois, J. Duprat, A. Korichi, N. Perrin, N. Poffé, H. Sergolle, J.F. Sharpey-Schafer, C.W. Beausang, S.J. Gale, M.J. Joyce, E.S. Paul, R.M. Clark, K. Hauschild, R. Wadsworth, J. Simpson, M.A. Bentley, A.G. Smith, H. Hübel, P. Willsau, G. DeFrance, I. Ahmad, M. Carpenter, R. Henry, R.V.F. Janssens, T.L. Khoo, T. Lauritsen, Z. Phys. A 348 (1994) 87.
[33] N. Fotiades, S. Harissopulos, C.A. Kalfas, S. Kossionides, C.T. Papadopoulos, R. Vlastou, M. Serris, M. Meyer, N. Redon, R. Duffait, Y. LeCoz, L. Ducroux, F. Hannachi, I. Deloncle, B. Gall, M.G. Porquet, C. Schück, F. Azaiez, J. Duprat, A. Korichi, J.F. Sharpey-Schafer, M.J. Joyce, C.W. Beausang, P.J. Dagnall, P.D. Forsyth, S.J. Gale, P.M. Jones, E.S. Paul, J. Simpson, R.M. Clark, K. Hauschild, R. Wadsworth, J. Phys. G: Nucl. Part. Phys. 21 (1995) 911.
[34] N. Fotiades, S. Harissopulos, C.A. Kalfas, S. Kossionides, C.T. Papadopoulos, R. Vlastou, M. Serris, J.F. Sharpey-Schafer, M.J. Joyce, C.W. Beausang, P.J. Dagnall, P.D. Forsyth, S.J. Gale, P.M. Jones, E.S. Paul, P.J. Twin, J. Simpson, D.M. Cullen, P. Fallon, M.A. Riley, R.M. Clark, K. Hauschild, R. Wadsworth, Z. Phys. A 354 (1996) 169.
[35] P. Wilsau, M. Neffgen, Y. LeCoz, H. Hübel, W. Korten, F. Hannachi, A. Korichi, M.G. Porquet, M. Kaci, N. Redon, M. Meyer, C.W. Beausang, E.S. Paul, J. Simpson, J.R. Hughes, Z. Phys. A 355 (1996) 129.
[36] M. Kaci, M.G. Porquet, I. Deloncle, M. Aiche, F. Azaiez, G. Bastin, C.W. Beausang, C. Bourgeois, R.M. Clark, R. Duffait, J. Duprat, B.J.P. Gall, F. Hannachi, K. Hauschild, M.J. Joyce, A. Korichi, Y. LeCoz, M. Meyer, E.S. Paul, N. Perrin, N. Poffé, N. Redon, C. Schück, H. Sergolle, J.F. Sharpey-Schafer, J. Simpson, A.G. Smith, R. Wadsworth, Nucl. Phys. A 697 (2002) 3.